Bioactive Glasses and Glass-Ceramics

Fundamentals and Applications

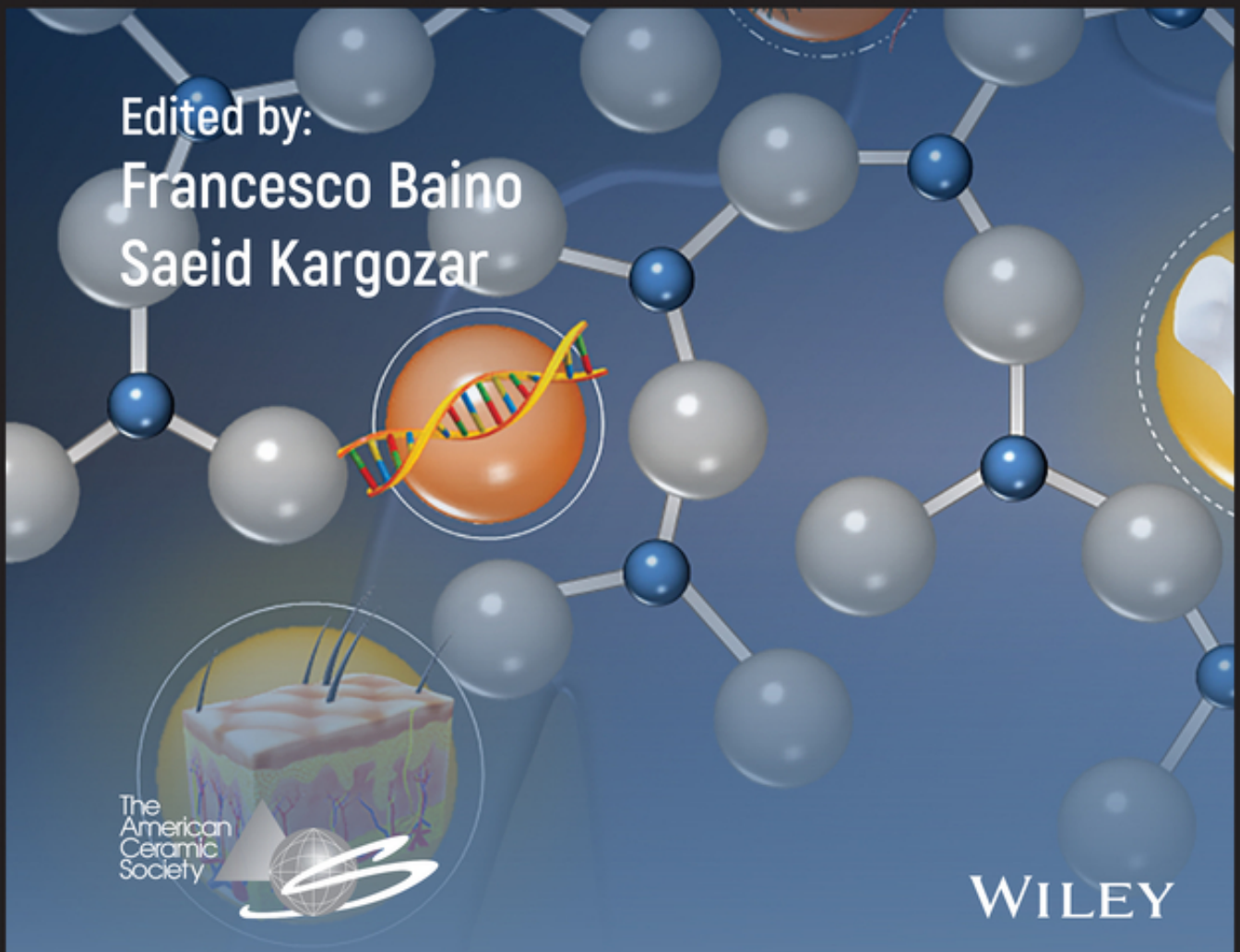

Edited by:
Francesco Baino
Saeid Kargozar

The American Ceramic Society

WILEY

Bioactive Glasses and Glass-Ceramics

Bioactive Glasses and Glass-Ceramics

Fundamentals and Applications

Edited by

Francesco Baino and Saeid Kargozar

WILEY

Published by John Wiley & Sons, Inc., Hoboken, New Jersey.

Published simultaneously in Canada.

Registered Office
John Wiley & Sons, Inc., 111 River Street, Hoboken, NJ 07030, USA

Editorial Office
111 River Street, Hoboken, NJ 07030, USA

For details of our global editorial offices, customer services, and more information about Wiley products visit us at www.wiley.com.

Wiley also publishes its books in a variety of electronic formats and by print-on-demand. Some content that appears in standard print versions of this book may not be available in other formats.

Library of Congress Cataloging-in-Publication Data

Names: Baino, Francesco, editor. | Kargozar, Saeid, editor.
Title: Bioactive glasses and glass-ceramics : fundamentals and applications / edited by Francesco Baino, Saeid Kargozar.
Description: Hoboken, New Jersey : Wiley-American Ceramic Society, [2022] | Includes bibliographical references and index.
Identifiers: LCCN 2022009994 (print) | LCCN 2022009995 (ebook) | ISBN 9781119724513 (cloth) | ISBN 9781119724889 (adobe pdf) | ISBN 9781119724667 (epub)
Subjects: LCSH: Bioactive glasses. | Glass-ceramics. | Glass in medicine. | Bioactive glasses–Therapeutic use. | Glass-ceramics–Therapeutic use.
Classification: LCC R857.G55 B544 2022 (print) | LCC R857.G55 (ebook) | DDC 610.28/4–dc23/eng/20220329
LC record available at https://lccn.loc.gov/2022009994
LC ebook record available at https://lccn.loc.gov/2022009995

Cover image: Courtesy Francesco Baino and Elisa Fiume
Cover design by Wiley

Set in 9.5/12.5pt STIXTwoText by Straive, Chennai, India

Contents

Preface

Bioactive glasses and glass-ceramics are a versatile class of biocompatible materials that have an astonishing impact in biomedicine. There is a long successful history in the synthesis, characterization, and utilization of these man-made materials. Generally, the expertise of researchers and scientists working in materials science, tissue engineering, biology, and medicine are required for producing the "best" glass and glass-ceramic formulations with optimized properties in favor of tissue repair and regeneration.

The first and foremost application of such biomaterials is addressed to treat hard tissue damages and injuries because of their inherent characteristics such as stiffness and bone-bonding ability. Bioactive glasses were first invented by Professor Larry L. Hench at the University of Florida more than half a century ago in 1969. The original bioactive glass, designed in a silicate system with a composition of $45SiO_2$–$24.5Na_2O$–$24.5CaO$–$6P_2O_5$ (wt%), was initially developed to meet the need for bone replacement of injured soldiers returned from the Vietnam War. Since then, a huge number of other compositions and bioactive glass-based products have been proposed and introduced into the market for managing hard tissue diseases and disorders. PerioGlas® and BonAlive® are two well-known synthetic bone grafts based on bioactive glasses with admirable success in the clinic. Over the last couple of decades, other types of bioactive glasses, including phosphate- and borate-based glasses, have been developed and applied for treating a wide range of tissue damages, including soft tissue injuries. In this regard, RediHeal™, a borate-based bioactive glass, is currently being used for managing wounds in animals and is awaiting for getting Food and Drug Administration (FDA) approval for practicing in humans suffering from slow-healing wounds (e.g. diabetic foot ulcers).

The main advantages of bioactive glasses are associated with their exceptional versatility in terms of composition–property relationships, controlled crystallized that can dictate the physicochemical and mechanical characteristics, and inherent ability to attach to both hard and soft tissues. Specifically, the ability to bond to living bone is related to the formation of a nano-crystalline hydroxyapatite layer, similar to bio-apatites, on the surface of bioactive glasses after exposure to body fluids. From a biological point of view, bioactive glasses cause no short- and long-term adverse effects on human cells, tissues, and organs; therefore, they are generally identified as biocompatible substances in biomedicine. Bioactive glasses are considered the osteoconductive and osteoinductive materials as they can provide a suitable substrate for adhesion and growth of bone-forming cells as well as induce osteoprogenitor cells to differentiate toward osteogenic lineages. In addition, bioactive glasses exhibit antibacterial, anti-inflammatory, and pro-angiogenic activities *in vitro* and *in vivo*. On this matter, a broad range of therapeutic ions (e.g. silver [Ag^+] and copper [Cu^{2+}]) are incorporated into the basic compositions of bioactive glasses to improve their biological performances imparting extra-functionalities, like antibacterial and pro-angiogenic properties. Indeed,

the release of therapeutic ions from bioactive glasses allows their usage as drug delivery vehicles for biomedical strategies. Recently published scientific reports emphasize the therapeutic capacity of bioactive glasses in battling against different types of cancers, especially those associated with hard tissues. On this point, mesoporous bioactive glasses possess an added value since their inherently nano-textured structure also provides a suitable platform for the incorporation and controlled delivery of a wide range of anti-cancer drugs to desired sites. With the advent of three-dimensional (3D) printing or additive manufacturing, the fabrication of 3D constructs based on or containing bioactive glasses and glass-ceramics offers a plethora of advantages, including improved mechanical strength and biological performance.

The present book aims to provide an updated understanding of biocompatible glasses and glass-ceramics based on current evidence in the literature and draw their future in the fields of biomaterials and tissue engineering. Basic aspects of bioactive glasses and glass-ceramics along with their fabrication routes and the latest processing strategies (e.g. additive manufacturing, laser treatments) are well-discussed from a materials science point of view. Besides, the biological effects of glasses and glass-ceramics have been considered on the living systems (*in vitro* and *in vivo*) as well as the current market needs and clinical challenges. The pros and cons of mesoporous bioactive glasses are argued in terms of drug delivery systems in relevant chapters. From a tissue engineering point of view, the regenerative capacity of different types of bioactive glasses and glass-ceramics has been reviewed in connection with hard (e.g. bone and teeth) and soft (e.g. skin) tissue healing. Moreover, hopes raised by these synthetic biomaterials in the treatment of malignancies have been well explored to shed light on their possible roles in the next-generation therapies. We hope that the present book is beneficial for the potential readership working in a broad community, who has a scientific background ranging from materials science and bioengineering to medicine and tissue engineering.

Politecnico di Torino, Turin, Italy — *Francesco Baino*
Mashhad University of Medical Sciences, Mashhad, Iran — *Saeid Kargozar*
March 26, 2022

List of Contributors

Simeon Agathopoulos
Department of Materials Science and Engineering
University of Ioannina
Ioannina
Greece

William Alles
Kazuo Inamori School of Engineering
Alfred University
Alfred, NY
USA

Felipe Arias-González
LaserON Laser Applications Research Group
Research Center in Technologies, Energy and Industrial Processes
CINTECX
University of Vigo
Vigo
Spain

and

Applied Physics Department
EEI, University of Vigo
Vigo
Spain

Mostafa Awaid
Department of Engineering
University of Rome "Niccolò Cusano", INSTM RU
Rome
Italy

Francesco Baino
Institute of Materials Physics and Engineering
Department of Applied Science and Technology (DISAT)
Politecnico di Torino
Torino
Italy

Sadaf Batool
School of Chemical and Materials Engineering (SCME)
National University of Sciences and Technology (NUST)
Islamabad
Pakistan

Stefano Berrettini
Laboratory of Temporal Bone Dissection and Otologic Tissue Engineering (OtoLab)
Department of Surgical, Medical, Molecular Pathology and Emergency Medicine
University of Pisa
Pisa
Italy

Aldo R. Boccaccini
Department of Materials Science and Engineering
Institute of Biomaterials
University of Erlangen-Nuremberg
Erlangen
Germany

Roger Borges
Centro de Ciências Naturais e Humanas
Universidade Federal do ABC
Santo André
Brazil

Mohamed Boutinguiza
LaserON Laser Applications Research Group
Research Center in Technologies, Energy and Industrial Processes
CINTECX
University of Vigo
Vigo
Spain

and

Applied Physics Department
EEI, University of Vigo
Vigo
Spain

Delia S. Brauer
Otto Schott Institute of Materials Research
Faculty of Chemistry and Earth Sciences
Friedrich Schiller University
Jena
Germany

Ilaria Cacciotti
Department of Engineering
University of Rome "Niccolò Cusano"
INSTM RU
Rome
Italy

Rafael Comesaña
LaserON Laser Applications Research Group
Research Center in Technologies, Energy and Industrial Processes
CINTECX
University of Vigo
Vigo
Spain

and

Department of Materials Engineering
Applied Mechanics and Construction
EEI, University of Vigo
Vigo
Spain

Glauco Cristofaro
Division of Otorhinolaryngology (ORL)
Arcispedale di "Santa Maria Nuova"
Florence
Italy

and

Laboratory of Temporal Bone Dissection and Otologic Tissue Engineering (OtoLab)
Department of Surgical, Medical, Molecular Pathology and Emergency Medicine
University of Pisa
Pisa
Italy

Serena Danti
Laboratory for Atomistic and Molecular Mechanics (LAMM)
Massachusetts Institute of Technology
Cambridge, MA
USA

and

University of Pisa Research Unit
National Interuniversity Consortium of Materials Science and Technology (INSTM)
Florence
Italy

and

Laboratory of Temporal Bone Dissection and Otologic Tissue Engineering (OtoLab)
Department of Surgical, Medical, Molecular Pathology and Emergency Medicine
University of Pisa
Pisa
Italy

and

Department of Civil and Industrial Engineering
University of Pisa
Pisa
Italy

Durgalakshmi Dhinasekaran
Department of Medical Physics
Anna University
Chennai
India

Konstantinos Dimitriadis
Department of Materials Science and Engineering
University of Ioannina
Ioannina
Greece

and

Division of Dental Technology
Department of Biomedical Sciences
University of West Attica
Athens
Greece

Ahmed El-Fiqi
Glass Research Department
Advanced Materials Technology and Mineral Resources Research Institute
National Research Centre
Cairo 12622
Egypt

Elisa Fiume
Institute of Materials Physics and Engineering
Department of Applied Science and Technology (DISAT)
Politecnico di Torino
Torino
Italy

Jessica Fletcher
Kazuo Inamori School of Engineering
Alfred University
Alfred, NY
USA

Qiang Fu
Science and Technology Division
Corning Inc.
Corning, NY
USA

Luis A. Genova
Centro de Ciência e Tecnologia dos Materiais
Instituto de Pesquisas Energéticas e Nucleares
São Paulo
Brazil

Smriti Gupta
Neurotherapeutics Laboratory
Department of Pharmaceutical Engineering and Technology
Indian Institute of Technology (Banaras Hindu University)
Varanasi
India

Leena Hupa
Johan Gadolin Process Chemistry Centre
Faculty of Science and Technology
Åbo Akademi University
Turku
Finland

Zakir Hussain
School of Chemical and Materials Engineering (SCME)
National University of Sciences and Technology (NUST)
Islamabad
Pakistan

Kanwal Ilyas
Department of Materials Science and Engineering
Institute of Biomaterials
University of Erlangen-Nuremberg
Erlangen
Germany

Giselle Z. Justo
Departamento de Bioquímica
Universidade Federal de São Paulo
São Paulo
Brazil

Saeid Kargozar
Tissue Engineering Research Group (TERG)
Department of Anatomy and Cell Biology, School of Medicine
Mashhad University of Medical Sciences
Mashhad
Iran

Timothy James Keenan
Kazuo Inamori School of Engineering
Alfred University
Alfred, NY
USA

Sairam Krishnamurthy
Neurotherapeutics Laboratory
Department of Pharmaceutical Engineering and Technology
Indian Institute of Technology (Banaras Hindu University)
Varanasi
India

Anuj Kumar
School of Chemical Engineering
Yeungnam University
Gyeongsan
Republic of Korea

Usman Liaqat
School of Chemical and Materials Engineering (SCME)
National University of Sciences and Technology (NUST)
Islamabad
Pakistan

Nina C. Lindfors
Department of Hand Surgery
Helsinki University Hospital
Helsinki
Finland

and

Department of Surgery
Helsinki University
Helsinki
Finland

Fernando Lusquiños
LaserON Laser Applications Research Group
Research Center in Technologies
Energy and Industrial Processes
CINTECX
University of Vigo
Vigo
Spain

and

Applied Physics Department
EEI, University of Vigo
Vigo
Spain

Joel Machado Jr.
Departamento de Ciências Biológicas
Universidade Federal de São Paulo
Diadema
Brazil

Shreyasi Majumdar
Neurotherapeutics Laboratory
Department of Pharmaceutical Engineering and Technology
Indian Institute of Technology (Banaras Hindu University)
Varanasi
India

Juliana Marchi
Centro de Ciências Naturais e Humanas
Universidade Federal do ABC
Santo André
Brazil

Jonathan Massera
Faculty of Medicine and Health Technology
Tampere University
Tampere
Finland

John C. Mauro
Department of Materials Science and Engineering
The Pennsylvania State University
University Park, PA
USA

Tina Mehrabi
Biomaterials Laboratory, Division of Biomedical Engineering
Department of Life Science Engineering
Faculty of New Sciences and Technologies
University of Tehran
Tehran
Iran

Abdorreza S. Mesgar
Biomaterials Laboratory, Division of Biomedical Engineering
Department of Life Science Engineering
Faculty of New Sciences and Technologies
University of Tehran
Tehran
Iran

Carla Migneco
Institute of Materials Physics and Engineering
Department of Applied Science and Technology (DISAT)
Politecnico di Torino
Torino
Italy

Mario Milazzo
Laboratory for Atomistic and Molecular Mechanics (LAMM)
Massachusetts Institute of Technology
Cambridge, MA
USA

University of Pisa Research Unit
National Interuniversity Consortium of Materials Science and Technology (INSTM)
Florence
Italy

and

Department of Civil and Industrial Engineering University of Pisa
Pisa
Italy

Zahra Mohammadi
Biomaterials Laboratory, Division of Biomedical Engineering
Department of Life Science Engineering
Faculty of New Sciences and Technologies
University of Tehran
Tehran
Iran

Maziar Montazerian
Department of Materials Engineering
Northeastern Laboratory for Evaluation and Development of Biomaterials (CERTBIO)
Federal University of Campina Grande
Campina Grande
Brazil

Araceli de Pablos Martín
Otto Schott Institute of Materials Research
Faculty of Chemistry and Earth Sciences
Friedrich Schiller University
Jena
Germany

Juan Pou
LaserON Laser Applications Research Group
Research Center in Technologies
Energy and Industrial Processes
CINTECX
University of Vigo
Vigo
Spain

and

Applied Physics Department
EEI, University of Vigo
Vigo
Spain

Félix Quintero
LaserON Laser Applications Research Group
Research Center in Technologies
Energy and Industrial Processes
CINTECX
University of Vigo
Vigo
Spain

and

Applied Physics Department
EEI, University of Vigo
Vigo
Spain

Antonio Riveiro
LaserON Laser Applications Research Group
Research Center in Technologies
Energy and Industrial Processes
CINTECX
University of Vigo
Vigo
Spain

and

Department of Materials Engineering
Applied Mechanics and Construction
EEI, University of Vigo
Vigo
Spain

Daniel J. Sola
Laboratorio de Óptica
Centro de Investigación en Óptica y Nanofísica
(CIOyN)
Campus Espinardo,
Universidad de Murcia
Murcia
Spain

and

Aragonese Foundation for Research and
Development (ARAID)
Government of Aragon
Zaragoza
Spain

Ana Carolina S. Souza
Centro de Ciências Naturais e Humanas
Universidade Federal do ABC
Santo André
Brazil

Dilshat U. Tulyaganov
Department of Natural–Mathematical Sciences
Turin Polytechnic University in Tashkent
Tashkent
Uzbekistan

Jesús del Val
LaserON Laser Applications Research Group
Research Center in Technologies
Energy and Industrial Processes
CINTECX
University of Vigo
Vigo
Spain

and

Applied Physics Department
EEI, University of Vigo
Vigo
Spain

Enrica Verné
Institute of Materials Physics and Engineering
Department of Applied Science and
Technology (DISAT)
Politecnico di Torino
Torino
Italy

Fabian Westhauser
Orthopedic University Hospital
Heidelberg
Germany

Sebastian Wilkesmann
Orthopedic University Hospital
Heidelberg
Germany

Collin Wilkinson
Department of Materials Science and
Engineering
The Pennsylvania State University
University Park, PA
USA

Anthony William Wren
Kazuo Inamori School of Engineering
Alfred University
Alfred, NY
USA

Seiji Yamaguchi
Department of Biomedical Sciences
College of Life and Health Sciences
Chubu University
Kasugai
Aichi
Japan

Min Zhu
School of Materials and Chemistry
University of Shanghai for Science and
Technology
Shanghai
PR China

Yufang Zhu
State Key Laboratory of High Performance
Ceramics and Superfine Microstructure
Shanghai Institute of Ceramics
Chinese Academy of Sciences
Shanghai
PR China

1

Glass Crystallization and Glass-Ceramics – An Overview

Araceli de Pablos Martín and Delia S. Brauer

Otto Schott Institute of Materials Research, Faculty of Chemistry and Earth Sciences, Friedrich Schiller University, Jena, Germany

1.1 Introduction

Glass-ceramics were first developed in 1952 by Stanley Donald Stookey, a glass researcher at Corning Glass Works. He realized that by controlled thermal treatment of the parent glass, it would be possible to transform a glass into a partially or fully crystalline material with new properties, which depend on the nature of the crystals formed [1–5] (and refs. therein).

Applications of glass-ceramics [6, 7] include technical applications, e.g. as photosensitive [8–10] or machinable glass-ceramics [11–13] (including magnesia aluminosilicate glass-ceramics [14]) or for radioactive waste immobilization [15–17]. Fresnoite glass-ceramics [18] have been shown to be very versatile in the technical field owing to their pyroelectric, piezoelectric as well as nonlinear optical properties. Glass-ceramics are also used in many consumer products. The heat resistance and very low coefficient of thermal expansion of lithium aluminosilicate (LAS) glass-ceramics make them ideal for use as cooker top panels, doors for fireplaces, and opaque and transparent cookware [19]. Transparent glass-ceramics based on nanocrystallization are employed as passive optical glass-ceramics, like telescope mirrors based on the LAS system, as well as active optical glass-ceramics, like oxyfluoride glass-ceramics, which are doped with lanthanide ions to achieve interesting optical properties [4, 20], e.g. up-conversion emission. Energy applications include ion-conducting glass-ceramics as components for lithium batteries and sealants for solid oxide fuel cells [21]. For architectural applications, the wollastonite glass-ceramic Neopariés® [3], used in construction, is a good example. In the biomedical field, glass-ceramics are used for bone replacement materials or as dental restoration [22–28].

Important glass-ceramics for biomedical applications, their crystalline phases, properties, and application are listed in Table 1.1. These glass-ceramics exhibit better mechanical properties than bioactive glasses, but their bioactivity is lower. Thus, a research aim in the 1990s was to develop a new glass-ceramic, combing the high bioactivity of Bioglass 45S5 with the good mechanical properties of the glass-ceramic Cerabone. The glass-ceramic Biosilicate, developed in 2007, fulfilled these requirements, highlighting the role of crystallization in both, bioactivity and mechanical properties [30, 33, 49].

Bioactive Glasses and Glass-Ceramics: Fundamentals and Applications, First Edition.
Edited by Francesco Baino and Saeid Kargozar.

Table 1.1 Selection of commercial bioactive glass-ceramics: composition, crystalline phases, crystallization mechanism and applications.

Composition (wt%)	Crystalline phases	Crystallization mechanism	Application	References
		Dicor		
56–64SiO_2 15–20MgO 12–18K_2O 4–9F 0.5ZrO_2	Mica ($K_2Mg_5Si_8O_{20}F_4$)	Internal crystallization from phase separation	Dentistry	[29]
		Ceravital		
40–50SiO_2 5–10Na_2O 30–35CaO 10–50P_2O_5 2.5–5MgO 0.5–3K_2O	Devitrite ($Na_2Ca_3Si_6O_{16}$) Ap	Internal crystallization	Replacing the ossicular chain (middle ear)	[30, 31]
		A/W Cerabone		
34.0SiO_2 4.6MgO 44.7CaO 16.2P_2O_5 0.5CaF_2	Ap Wollastonite ($CaSiO_3$)	Surface crystallization (from the surfaces of glass particles)	Bone replacement (e.g. iliac crest)	[25, 32]
		Biosilicate		
48.5SiO_2 23.75Na_2O 23.75CaO 4P_2O_5	$Na_2CaSi_2O_6$ or $Na_2CaSi_2O_6$ and $NaCaPO_4$ (depending on the thermal conditions)	Internal crystallization	Orthopedics, dentistry, treatment of dental hypersensitivity	[30, 33–38]
		Bioverit I		
5.5–9.5Na_2O/K_2O 13–28CaO 6–28MgO 0–19.5Al_2O_3 29.5–50SiO_2 8–18P_2O_5 2.5–7F some TiO_2	Fluorophlogopite mica ($Na/KMg_3(AlSi_3O_{10}F_2)$) Ap	Internal crystallization from phase separation droplets	Orthopedics, head and neck surgery	[32, 39]
		Bioverit II		
7–10.5Na_2O/K_2O 0.1–3CaO 11–15MgO 26–30Al_2O_3 43–50SiO_2 0.1–5P_2O_5 3.3–4.8F	Fluorophlogopite mica ($Na/KMg_3(AlSi_3O_{10}F_2)$) Cordierite ($Mg_2Si_5Al_4O_{18}$)	Internal crystallization from phase separation droplets	Orthopedics, head and neck surgery	[32, 39–43]

(Continued)

Table 1.1 (Continued)

Composition (wt%)	Crystalline phases	Crystallization mechanism	Application	References
		Lithium silicate glass-ceramics		
Li_2O–K_2O–Al_2O_3–SiO_2–(ZnO)	Li_2SiO_3 $Li_2Si_2O_5$ Li_3PO_4 Depending on the composition	Internal crystallization	Dentistry	[44–47]
		Bioverit III		
45–44P_2O_5 6–18Al_2O_3 3–19CaO 11–18Na_2O 1.5–10 Additional agents	Ap Berlinite ($AlPO_4$) Varulite-like type (Na–Ca–Fe phosphate)	Internal crystallization	Orthopedics	[39, 40]
		IPS d.SIGN®		
50–65SiO_2 8–20Al_2O_3 7–13K_2O 4–12Na_2O 0.1–6CaO 0–5P_2O_5 0.1–3F 0–3 Additional agents	Leucite ($KAlSi_2O_6$) Ap $NaCaPO_4$	Surface crystallization of Leucite. Internal crystallization of Ap and $NaCaPO_4$ from phase separation	Dentistry	[48]

Ap: (Fluor)Apatite.

1.2 Controlled Crystallization of Glasses

Glass-ceramics are prepared by controlled heat treatment of glasses. When discussing crystallization of glasses, two different sequences must be distinguished: (i) spontaneous and uncontrolled crystallization occurring during cooling of the melt, which is an undesired event and typically leads to poor mechanical properties of the final material, and (ii) controlled crystallization by performing a single or successive heat treatments on a glass by following a well-defined time–temperature protocol, obtaining the desired crystalline fractions, crystal sizes, and morphologies. The process is described in several reviews [6, 50–53]. Controlled heat treatment allows us to obtain *glass-ceramics*. In 2017, technical committee TC07 of the International Commission on Glass (ICG), dedicated to crystallization and glass-ceramics, published an updated definition of glass-ceramics, considering current advanced preparation routes, new compositional families, a broader range of crystalline fractions, and including both surface and bulk crystallization [54]. Thus, a more complete definition was proposed: "Glass-ceramics are inorganic, non-metallic materials prepared by controlled crystallisation of glasses via different processing methods. They contain at least one type of functional crystalline phase and a residual glass. The volume fraction crystallised may vary from ppm to almost 100%." (Bioactive) Glass-ceramics are typically

prepared by (i) conventional melting and thermal treatment of the parent glass; (ii) sintering and crystallization of glass powders, or (iii) by sol–gel technology, which is an interesting example for the development of new coatings of orthopedic metallic implants (such as Ti-based alloys) to improve their integration with the host tissue and facilitate bone induction and cell proliferation [55–57]. It is also possible to prepare glass-ceramics by simultaneous sintering and crystallization of glass powder compacts with or without dopants to stimulate local tissue repair [25, 58].

Crystallization is an exothermic process and occurs in two stages: first, at temperatures slightly above the glass transition, *nucleation* takes place. The second stage, *crystal growth*, takes place at higher temperatures to promote the growth of those nuclei. The time necessary to develop the desired crystal fraction, including crystal size, depends on well-defined nucleation (I) and crystal growth (U) rates at a given temperature. The crystallization process is framed in the classical nucleation theory (CNT) [50, 52, 53, 59, 60], which is still being updated [6, 61–65].

1.3 Nucleation

The atoms in a glass constantly vibrate owing to their inherent thermal energy. Given the right circumstances of compositional fluctuations, temperature (below *liquidus* T_L), and time, individual structural units can join to form a nucleus of critical size, with radius r^*. This will be the precursor of a crystal with further heat treatment. Below the critical size r^* the nuclei are not stable and dissolve in the glassy matrix. In order to cover the whole r range, from nonstable embryos to stable nuclei above the critical size, we will refer to *clusters*.

Nucleation can be *homogeneous* (HOM) or *heterogeneous* (HET), depending on the existence of nucleation sites [63, 66]. Table 1.2 summarizes the most important features of both mechanisms [63, 66, 67].

The equations needed to calculate the thermodynamic and kinetic parameters of nucleation and crystallization are very usefully summarized in some publications [62, 68–71]. Assuming a spherical cluster, the variation of the free energy associated to the cluster formation can be expressed as a

Table 1.2 Differences between homogeneous (HOM) and heterogeneous (HET) nucleation.

HOM	HET
Main characteristics	
Nucleation without nucleation sites	Presence of nucleation sites
Nucleation starts in the volume of the glass and the probability of nucleation is equal everywhere	Nucleation can start in the volume (through the addition of nucleating agents) or at the surface (through foreign species). It can enable epitaxial growth
Variables	
Temperature, time, pressure	Temperature, time, pressure, specific energy, chemical gradients, stresses
Free energy for the formation of a critical size nucleus, ΔG^*	
$\Delta G^*(\mathrm{HOM}) = \frac{16\pi\sigma^3}{3\Delta G_V^2}$	$\Delta G^*(\mathrm{HET}) = \Delta G^*(\mathrm{HOM}) \cdot \left[\frac{(1-\cos\theta)^2 \cdot (2+\cos\theta)}{4}\right]$

θ is the contact angle of the nuclei species at the surface of the active sites ($\theta = 180°$ for HOM, $\theta < 180°$ for HET), σ is the free energy per unit area of crystal/glass interface, and ΔG_V is the free energy change per unit volume of crystals.

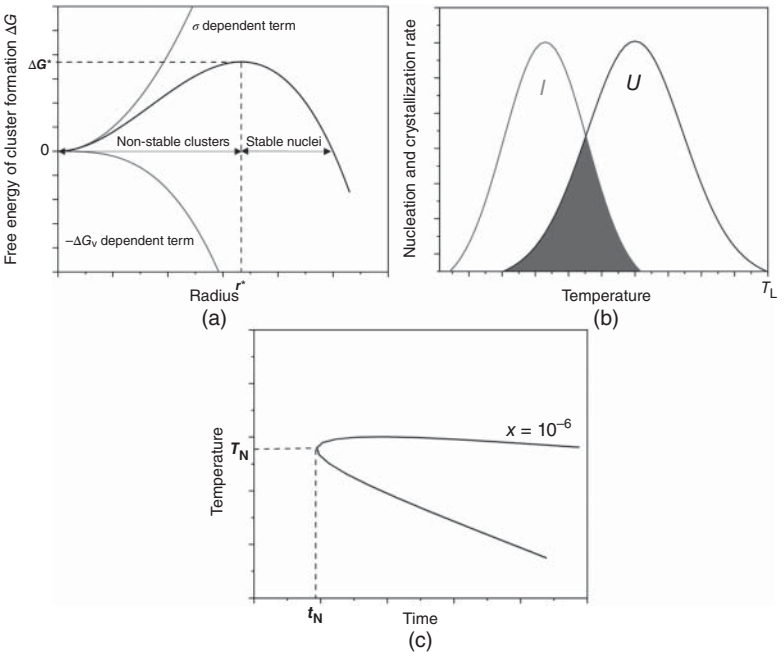

Figure 1.1 (a) Schematic representation of the free energy for cluster formation, ΔG, as a function of cluster size r. ΔG^* and r^* are the thermodynamic barrier for nucleation and critical cluster size, respectively. (b) Schematic illustration of Tammann's curves, showing nucleation and crystallization rates, I and U. The overlapping area of both curves (shaded in grey) usually gives the interval of crystallization. (c) Sketch of a TTT curve for a crystallized volume fraction of $x = 10^{-6}$. Nose temperature and the corresponding time are indicated as T_N and t_N, respectively.

function of its radius r. This variation of free energy is represented as the sum of two contributions (Eq. (1.1)):

$$\Delta G = \frac{4}{3}\pi r^3 \Delta G_V + 4\pi r^2 \sigma \tag{1.1}$$

which contains a volume-dependent term (cubed dependence with radius, r^3) and a surface-dependent term (squared dependence with radius, r^2) (Figure 1.1a). The former represents the energy decrease on ordering an amorphous region to form a crystalline lattice, and it is given by the volume $V = 4\pi r^3/3$ (for a spherical cluster) multiplied by the free energy of crystallization per unit volume, ΔG_V. The second term is surface-dependent, and it is associated with the energy involved to form a new spherical surface of solid/liquid interfacial area $4\pi r^2$, i.e. the crystal/liquid interfacial free energy, σ, which can be estimated [68]. The free energy of crystallization, ΔG_V, depends on the undercooling, $\Delta T = T - T_L$, according to $\Delta G_V = \Delta T\, L/T_L$, where T_L is the liquidus temperature, T is a given nucleation temperature and L is the latent heat of fusion per unit volume. ΔG_V is negative ($\Delta G_V = G_{V(crystal)} - G_{V(amorphous)}$), since the forming nucleus has a lower Gibbs free energy than the undercooled liquid for $T < T_L$. The actual *driving force for nucleation* is ΔG_V. Figure 1.1a shows schematically the plot of ΔG as a function of r (Eq. (1.1)). For low values of r, the square term dominates over the cubic term, so that ΔG initially increases until a maximum and then decreases, when the volume-dependent term dominates. The maximum of the curve of ΔG vs. r corresponds to the critical radius r^*, where $d\Delta G = 0$. Deriving Eq. (1.1) and equaling zero, the

critical radius r^* is given by

$$r^* = \frac{-2\sigma}{\Delta G_V} \tag{1.2}$$

Note that ΔG_V is negative and, thus, r is a positive value. Substituting in the volume term of Eq. (1.1),

$$\Delta G^* = \frac{16\pi\sigma^3}{3(\Delta G_V)^2} \tag{1.3}$$

where ΔG^* (or W^* in some publications) represents the energy to overcome the nucleation barrier, i.e. the *free energy for the formation of a critical size nucleus* (Figure 1.1a). From Eq. (1.3), the strong (square) dependence of ΔG^* on the temperature is clear (since $\Delta G_V = \Delta T\, L/T_L$). Thus, the ΔG curve (Figure 1.1a) will vary depending on the nucleation temperature [62]. Considering that $\Delta G = \Delta G_V \cdot V_m$ and $\Delta G = (\Delta H_m \cdot \Delta T)/T_m$ (V_m is the molar volume of the crystalline phase, ΔH_m is the melting enthalpy per mole, ΔT is the undercooling, and T_m is the melting temperature), and substituting ΔG_V in Eq. (1.3), a more practical expression of ΔG^* is given [68]:

$$\Delta G^* = \frac{16\pi\sigma^3 V_m^2 T_m^2}{3\Delta H_m^2 \Delta T^2} \tag{1.4}$$

It is worth noting that r^* (Eq. (1.2)) and ΔG^* (Eq. (1.3)) decrease with increasing the degree of undercooling, ΔT, i.e. with decreasing temperature. At very high temperatures (small undercooling ΔT) r^* would be so large that it would not be possible to form a stable nucleus (note that for the extreme case of $\Delta T = 0$ the values of r^* and ΔG^* become infinite, Eqs. (1.2) and (1.4)). Moreover, this would imply that all glasses should be able to nucleate at temperatures well below T_L (because of the very low thermodynamic barrier ΔG^*), which does not agree with the experimental results. Thereof, kinetic considerations must be taken into account.

Considering the kinetic aspect of the nucleation, the rate at which the nuclei will appear in the glass at a given temperature is given by the steady-state nucleation rate, I (nuclei/m^3 s):

$$I = A\, \exp\left(-\frac{\Delta G^* + \Delta G_D}{kT}\right) \tag{1.5}$$

where A is a preexponential factor, $A = n_v \cdot kT/h$, h is the Planck constant and n_v is the number of atoms per unit volume, $n_v = N_A/V_m$ [68], and represents the probability of formation of a nucleus of critical size ($<10^{13}$ s^{-1} m^{-3} for HOM nucleation of silicate glasses [62]). $\Delta G^*/kT$ (or W^*/kT) and $\Delta G_D/kT$ (k is the Boltzmann constant) in Eq. (1.5) represent the thermodynamic and the diffusion barriers for the formation of a critical size nucleus and for diffusion (of atoms toward the nucleus interface), respectively.

The kinetic barrier, $\Delta G_D/kT$, can be expressed considering the atomic jump distance, λ, and the diffusion coefficient, $D = kT/\lambda\eta$, [62] as follows:

$$\frac{\Delta G_D}{kT} = \ln\left(\frac{kT\lambda^2}{hD}\right) \tag{1.6}$$

ΔG^* increases with increasing (nucleation) temperature (Eq. (1.4)), and thus, I increases until a maximum, which is close to the glass transition temperature, T_g, of the glass (Figure 1.1b). A detailed study of the relationship between the temperature of maximum nucleation rate and the T_g is reported in [72]. At temperatures lower than the temperature of maximum nucleation rate, ΔG_D dominates in Eq. (1.5), and nucleation becomes slower (I decreases), owing to an increase of viscosity (diffusion coefficient D decreases) and the associated limited atomic mobility with decreasing temperature from T_g (Figure 1.1b).

A very useful example of how the thermodynamic parameters of the nucleation process are calculated is found in the paper by Cabral et al. [68], where I, ΔG^*, ΔG_V, and σ are represented as a function of temperature for fresnoite glass. In practice, I can be also determined from the plot of the nucleus number density (N_v, nuclei/m^3) as a function of time of treatment at a fixed nucleation temperature. N_v is determined from optical or scanning microscopy experiments using image analysis software, by counting the number of nuclei per unit of area [73], or even through thermal analysis [74]. At the beginning of a nucleation treatment N_v increases quasi exponentially with time, then a linear increase of N_v takes place, which is the stationary nucleation regime. The nucleation rate, I (nuclei/m^3 s), corresponds to the slope of that straight segment. An interesting example for a high value of nucleation rate is that of fresnoite glass, which exhibits one of the highest nucleation rates (10^{17} m^{-3} s^{-1}) measured in inorganic glasses [68, 75]. Nucleation rates of $Li_2O{\cdot}SiO_2$ and $Na_2O{\cdot}2CaO{\cdot}3SiO_2$ glasses have been also determined [70, 73].

Experimentally, an estimation of the temperature of maximum nucleation can be obtained from thermal analysis [74]. Plotting the crystallization temperatures of differential scanning calorimetry (DSC) curves (crystallization peak, T_c) as a function of different nucleation temperatures, a curve will be obtained, whose minimum is the most effective nucleation temperature.

For the two mechanisms of nucleation (Table 1.2), the energy for critical cluster formation is usually lower in HET than in HOM, since nucleation is facilitated (catalyzed) in the presence of a crystalline primary nucleus in the former. Moreover, in HET, the interfacial energy (Eq. (1.1)) is reduced. These active nucleation sites can be nucleating agents intentionally added to the composition for this purpose (typical examples are TiO_2, ZrO_2, Fe_2O_3, Au, Ag, Pt, or Pd), or it may happen in an undesired/uncontrolled way through impurities, bubbles, foreign species on the container walls or in the atmosphere, etc. The main condition for HET to take place is proper wettability of the primary nucleus with the nucleating sites, which is given by the contact angle Θ. HET is particularly effective if the lattice parameters of crystal and nucleating site (in at least two directions) do not differ by more than 15%, which is called *epitaxial growth*. Table 1.2 displays the thermodynamic barrier for formation of a critical size (r^*) nucleus (ΔG^*) for both mechanisms. Nucleation rates of both mechanisms can be determined experimentally [71].

As part of the nucleation stage, *phase separation* (PS) phenomena in glasses must be considered. Although PS phenomena are inevitably associated with a source of defects in industrial glass production (mainly loss of transparency), for the preparation of glass-ceramics by controlled crystallization may be considered as an advantage. PS can have two different mechanisms: *nucleated* and *spinodal*. For the purpose of this chapter, only nucleated PS will be discussed. Usually, PS droplets are enriched in network modifiers, while the glassy matrix becomes enriched in SiO_2 or other network formers [19]. In a phase-separated base glass, nucleating agents may accumulate in one of the microphases [66]. These compositional fluctuations inevitably affect the kinetic of nucleation. Recently, Zanotto reviewed the aspects of PS influence in crystallization [76]. As reported, PS leads to a higher thermodynamic driving force, an increase in the diffusion of atoms, also increasing the nucleation rate, and lowering the interfacial energy, σ. Various N_v vs. time curves of phase-separated glasses were reviewed. For many years, it was believed that PS droplets act as active sites for nucleation in the volume of the glass, favoring internal crystallization. However, according to Zanotto [76], PS acts in a different way, in which PS shifts the composition of the glass matrix toward that of the stoichiometric crystal phase, increasing the crystal nucleation rate, which is actually the real effect rather than the presence of nucleation sites. New insight into the role and development of PS droplets in glass-ceramics has been obtained in the last years thanks to the availability of latest generation transmission electron microscopes. The work by Höche and coauthors is worth mentioning here [19, 77–82].

1.4 Crystal Growth

Once the nuclei have reached the critical size (r^*), they are able to grow to form crystals through deposition of atomic layers. Similar to the nucleation process, this stage is characterized by the crystal growth nucleation rate, U, which also contains a thermodynamic and a kinetic barrier. The kinetic term is governed by the diffusion of atoms, which are joined with the growing crystal (proportional to the activation energy for diffusion ΔG_D), but also those which are detached and return to the liquid (proportional to $\Delta G_D + \Delta G_V$). Considering these two contributions, the net crystal growth rate is expressed by:

$$U = f\lambda\frac{kT}{h}\exp\left(\frac{-\Delta G_D}{kT}\right)\left(1-\exp\left(\frac{\Delta G_V}{kT}\right)\right) \tag{1.7}$$

where f is the fraction of sites on the interface where the atoms are preferentially attached or removed, and can be determined experimentally [83], λ is the diffusion distance or distance advanced by the interface (usually taken as a molecular diameter) [83], and η is the shear viscosity. The diffusion coefficient of the Stokes–Einstein/Eyring equation: $D = kT/\lambda\eta$ is implicit in Eq. (1.7) through Eq. (1.6). Note that the diffusion in the crystal growth stage is not necessarily the same as for the nucleation stage, since the diffusion of the atoms during nucleation is more local (over smaller distances) than during the crystal growth stage. A very useful description of the role of the diffusion coefficient in the crystal growth has been published [84]. Note that at T_L (undercooling $\Delta T = 0$), $\Delta G_V = 0$ and $U = 0$ (Figure 1.1b). Lowering the temperature from T_L (increasing undercooling) leads to an increase in the crystal growth rate U until a maximum is reached. Similarly to the nucleation rate I, when the diffusion term governs at low temperatures and approaches zero, the crystal growth rate U decreases (Figure 1.1b).

In practice, and similar to I, U can be also determined from plots of size (or radius) of crystals (determined by microscopy or from X-ray diffraction analyses using the Scherrer equation) as a function of treatment time at a fixed temperature. The slope of the straight line is the crystallization rate U (μm/min) [75].

Moreover, the time dependence of the crystal size (r) can be fitted according to $r = U \cdot t^p$, where r is the average crystal radius, U is the growth rate, t is the dwell time of the heat treatment, and p is the growth exponent [85].

When preparing (bioactive) glass-ceramics, controlled heat treatment is usually performed below liquidus temperature. U usually increases with temperature until a maximum (Figure 1.1b). At higher temperatures than that of the maximum, the crystal growth rate decreases, owing to the difficulty of dissipating the heat from the crystallization process. At lower temperatures, high viscosity hinders crystal growth. Thus, the role of viscosity (and thus, diffusion) is key to improve and update nucleation and crystal growth equations [61, 83, 86–88].

If nucleation and crystal growth rates (I and U) are plotted together as a function of temperature (Tammann's curves [51, 62]), it is obvious that the maximum of I occurs at lower temperatures than that of U. The overlapping of both curves usually gives the interval of crystallization, in the way that the larger the overlap, the higher the crystallization tendency [89] (Figure 1.1b).

In a typical double-stage heat treatment, where nucleation treatment is carried out first and then crystal growth treatment follows at higher temperature (this is carried out when the I and U curves overlap only minimally or not at all), the kinetics of both processes are key for the development of glass-ceramics. The kinetic dependence [71, 90, 91] can be described through the following time parameters: an initial time, t_0, which is the time at which the first structural units are experimentally detected, and which corresponds to the first experimental point of the N_v vs. time curve; the

induction time, t_{ind}, which in the N_v vs. time curve comprises the time between $t = 0$ and the interception of the straight line with the time axis [70, 73]. The induction time, t_{ind}, is in fact the sum of three contributions [91]: *time lag*, τ, which is the period of time in which the size of the nuclei grows until r^* ($r \leq r^*$ regime), the average time of formation of the first supercritical nucleus in the steady-state nucleation regime, t_{ss} [91], and *incubation time*, t_i, which is the time required by the nuclei/crystals to grow to a detectable size and, of course, depends on the temperatures of the nucleation and crystal growth processes [91]. Moreover, the heating rate of the heat treatment plays a significant role in the kinetics of nucleation and crystal growth, as discussed by Deubener et al. [91], since the induction time, t_{ind}, increases with increasing heating rates with a cubic root dependence.

From a practical point of view, thermal characterization techniques, like DSC [74, 92], heating microscopy, or viscometry [93], also in combination with optical and electron microscopy nucleation studies, are widely employed to determine the thermodynamics and kinetics of crystallization in glasses. Good examples are the studies by the groups of Zanotto and Deubener, among others [62, 63, 74, 83, 84, 86–88, 91].

Time–temperature–transformation curves (TTT curves) are a very useful representation of the crystallization process [54, 71] (Figure 1.1c). A very illustrative use of TTT curves is for the determination of the minimum cooling rate necessary to form a glass (without crystallization occurring), which is the *critical cooling rate*, q_c. Uncontrolled crystallization upon cooling of the glass melt can be avoided if cooling is rapid enough (there is no time for reorganization of atoms to form ordered structures). The critical cooling rate can be determined from the TTT curve for transformation (crystals concentration) $x = 10^{-6}$ (1 ppm), which is assumed to be the detection limit by conventional experimental techniques. The critical cooling rate is then $q_c = (T_L - T_N)/t_N$, where T_N is the "nose temperature" of the TTT curve, which corresponds to the temperature at which the time to achieve a crystal fraction of 10^{-6} is the shortest (shortest time, t_N) [54, 71] (Figure 1.1c).

Related to the HOM and HET classification, crystallization can be also classified as *internal* (also called volume or bulk crystallization) or *surface crystallization* [94], depending on where the nuclei formation starts. Although most glasses undergo internal crystallization (HOM or HET) [22, 30], some well-known glass-ceramics which crystallize following a surface crystallization mechanism are cordierite ($2MgO{\cdot}2Al_2O_3{\cdot}5SiO_2$), diopside ($MgO{\cdot}CaO{\cdot}2SiO_2$), and devitrite ($Na_2O{\cdot}3CaO{\cdot}6SiO_2$) glass-ceramics, which are obtained from stoichiometric or near-stoichiometric glass compositions [95] (and refs. therein). Moreover, a third possibility exists, since surface and bulk crystallization may occur simultaneously (even competing) (Figure 1.2) [64, 97]. Table 1.1 displays some of the bioactive glass-ceramic systems showing internal or surface crystallization, or a combination of both.

Although it can occur in bulk pieces, surface crystallization is the predominant mechanism in powders, owing to the larger relative surface area. Thus, its study is particularly important when the bioactive glass-ceramics are intended to be used as powders, particulates, or slurries [98] or as scaffolds obtained by sintering of glass powders. By contrast, internal crystallization of bioactive glass-ceramics must be investigated when bulk pieces are used for application as monoliths. Unlike glass powders, bulk pieces can be machined to specific geometries. As a combination of both, powder compacts can be prepared by sintering of glass powders as well. Here, surface crystallization takes place at the surface of the powder grains, while internal nucleation may occur in the interior of the grains. Whether powder or bulk material are used depends on the final application.

The influence of the heat treatment on glass-ceramic microstructure is illustrated in Figure 1.2, using leucite-apatite glass-ceramics as an example [48, 64, 96, 99]. Leucite crystals form at the surface and grow dendritically into the bulk, as shown in a cross-section micrograph in [48]. Apatite crystals are formed in the bulk of the glass-ceramic, and their morphology can be tuned from droplets to needles, depending on the heat treatment (Figure 1.2) [64].

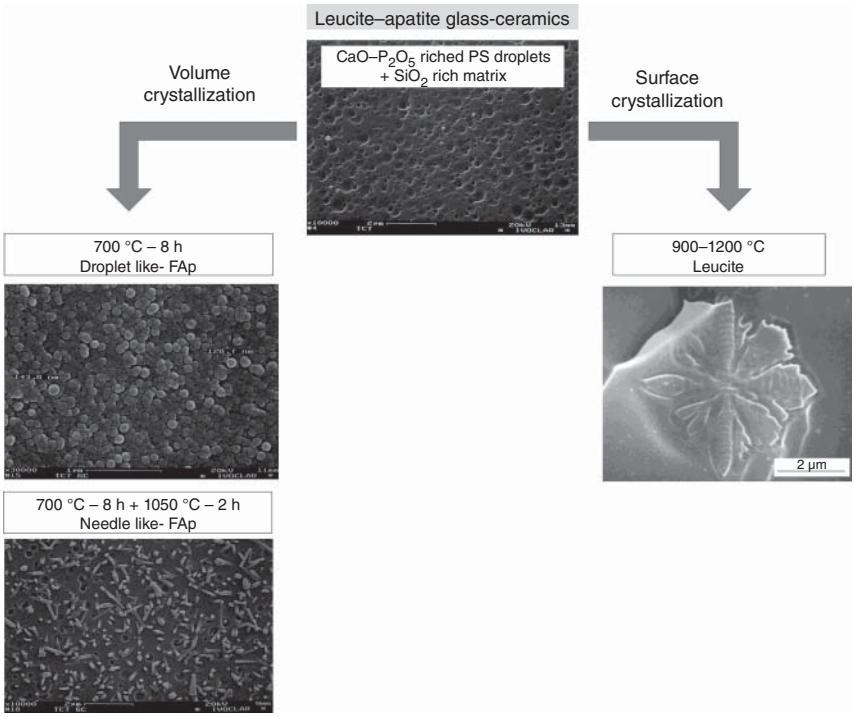

Figure 1.2 Scheme of leucite-apatite glass-ceramics, showing the crystallization of leucite at the surface (right) and that of fluorapatite (FAp) in two different morphologies in the volume (left). Source: Micrographs of the phase separated glass, droplet like- and needle like-FAp are from Höland et al. [64], with permission of Elsevier. Micrograph of the surface crystallization of leucite is from Höland et al. [96], Figure 03, p. 03/with permission of John Wiley & Sons, Inc.

1.5 Conclusion

Glass-ceramics offer the possibility to fine-tune crystal phase, size and fraction, and, ultimately, the bioactivity of a material via heat treatment. This illustrates the relevance and possible impact of crystallization for bioactive glass-ceramics, but it also shows that for these materials a broader range of applications may be possible than for the precursor parent glasses. If we know the main parameters governing nucleation and crystallization processes in glasses and understand the influence of temperature, diffusion, viscosity, phase separation or nucleating agents, a successful temperature–time protocol can be established to obtain the desired microstructure. This makes it possible to prepare (bioactive) glass-ceramics which meet the requirements for a particular clinical application.

References

1 Beall, G.H. and Pinckney, L.R. (1999). Nanophase glass-ceramics. *Journal of the American Ceramic Society* 82: 5–16.

2 Stookey, S.D. (2000). *Explorations in Glass: An Autobiography*. Wiley.

3 Zanotto, E.D. (2010). A bright future for glass-ceramics. *American Ceramic Society Bulletin* 89: 19–27.
4 De Pablos-Martin, A., Ferrari, M., Pascual, M.J., and Righini, G.C. (2015). Glass-ceramics: a class of nanostructured materials for photonics. *La Rivista del Nuovo Cimento* 38: 311–369.
5 Hench, L.L. (2011). Glass and glass-ceramic technologies to transform the world. *International Journal of Applied Glass Science* 2: 162–176.
6 Höland, W. and Beall, G.H. (2012). *Glass-Ceramic Technology*. Wiley.
7 Davis, M.J. and Zanotto, E.D. (2017). Glass-ceramics and realization of the unobtainable: property combinations that push the envelope. *MRS Bulletin* 42: 195–199.
8 Borrelli, N.F. (2016). *Photosensitive Glass and Glass-Ceramics*. CRC Press.
9 Stoica, M., Patzig, C., Bocker, C. et al. (2017). Structural evolution of CaF_2 nanoparticles during the photoinduced crystallization of a Na_2O–K_2O–CaO–CaF_2–Al_2O_3–ZnO–SiO_2 glass. *Journal of Materials Science* 52: 13390–13401.
10 Nascimento, M.L.F. (2016). Centenary of a serendipitous inventor: Stookey and a short statistical overview of photosensitive glass & glass-ceramics science and technology. *Recent Patents on Materials Science* 9: 33–44.
11 Henry, J., Chen, X., Law, R.V., and Hill, R.G. (2018). The investigation of the crystalline phases development in Macor® glass-ceramic. *Journal of the European Ceramic Society* 38: 245–251.
12 Guedes, A., Pinto, A.M.P., Vieira, M., and Viana, F. (2001). Multilayered interface in Ti/Macor® machinable glass-ceramic joints. *Materials Science and Engineering A* 301: 118–124.
13 Höland, W. and Vogel, W. (2013). Machinable and phosphate glass-ceramics. In: *An Introduction to Bioceramics*, 2e (ed. L.L. Hench), 215–228. World Scientific Publishing Company.
14 Benitez, T., Veber, A., Pagnan Furlan, K. et al. (2020). Development of magnesium-aluminum-silicate glass-ceramics nucleated with Nb_2O_5. *International Journal of Applied Glass Science* 11: 155–169.
15 Cao, C. and Goel, A. (2016). Apatite based ceramic waste forms for immobilization of radioactive iodine, an overview – 16155. *WM2016 Conference, March 6 – 10, 2016, Phoenix, Arizona, USA*, WM Symposia.
16 Ojovan, M.I. and Batyukhnova, O.G. (2007). Glasses for nuclear waste immobilization. In: *WM '07 Conference, Tucson, AZ, USA*, 15. WM Symposia.
17 Donald, I.W., Metcalfe, B.L., and Taylor, R.N.J. (1997). The immobilization of high level radioactive wastes using ceramics and glasses. *Journal of Materials Science* 32: 5851–5887.
18 Wisniewski, W., Thieme, K., and Rüssel, C. (2018). Fresnoite glass-ceramics – a review. *Progress in Materials Science* 98: 68–107.
19 Kleebusch, E., Patzig, C., Höche, T., and Rüssel, C. (2018). The evidence of phase separation droplets in the crystallization process of a Li_2O–Al_2O_3–SiO_2 glass with TiO_2 as nucleating agent – an X-ray diffraction and (S)TEM-study supported by EDX-analysis. *Ceramics International* 44: 2919–2926.
20 Berneschi, S., Soria, S., Righini, G.C. et al. (2010). Rare-earth-activated glass-ceramic waveguides. *Optical Materials* 32: 1644–1647.
21 de Pablos-Martin, A., Rodriguez-Lopez, S., and Pascual, M.J. (2020). Processing technologies for sealing glasses and glass-ceramics. *International Journal of Applied Glass Science* 11: 552–568.
22 Fu, L., Engqvist, H., and Xia, W. (2020). Glass-ceramics in dentistry: a review. *Materials* 13: 1049.
23 Pollington, S. (2011). Novel glass-ceramics for dental restorations. *Journal of Contemporary Dentistry* 12: 60–67.

24 Kasuga, T. (2007). Development of phosphate glass-ceramics for biomedical applications. *Journal of the Ceramic Society of Japan* 115: 455–459.

25 Kokubo, T. (1991). Bioactive glass ceramics: properties and applications. *Biomaterials* 12: 155–163.

26 Fernandes, H.R., Gaddam, A., Rebelo, A. et al. (2018). Bioactive glasses and glass-ceramics for healthcare applications in bone regeneration and tissue engineering. *Materials* 11: 2530.

27 Jones, J.R., Brauer, D.S., Hupa, L., and Greenspan, D.C. (2016). Bioglass and bioactive glasses and their impact on healthcare. *International Journal of Applied Glass Science* 7: 423–434.

28 Jones, J.R. (2013). Review of bioactive glass: from hench to hybrids. *Acta Biomaterialia* 9: 4457–4486.

29 Bapna, M.S. and Mueller, H.J. (1996). Study of devitrification of Dicor® glass. *Biomaterials* 17: 2045–2052.

30 Crovace, M.C., Souza, M.T., Chinaglia, C.R. et al. (2016). Biosilicate® – a multipurpose, highly bioactive glass-ceramic. In vitro, in vivo and clinical trials. *Journal of Non-Crystalline Solids* 432: 90–110.

31 Ohtsuki, C., Kushitani, H., Kokubo, T. et al. (1991). Apatite formation on the surface of Ceravital-type glass-ceramic in the body. *Journal of Biomedical Materials Research* 25: 1363–1370.

32 Montazerian, M. and Dutra Zanotto, E. (2016). History and trends of bioactive glass-ceramics. *Journal of Biomedical Materials Research Part A* 104: 1231–1249.

33 Moura, J., Teixeira, L.N., Ravagnani, C. et al. (2007). In vitro osteogenesis on a highly bioactive glass-ceramic (Biosilicate®). *Journal of Biomedical Materials Research Part A* 82: 545–557.

34 Azenha, M.R., Peitl, O., and Barros, V.M.R. (2010). Bone response to biosilicates® with different crystal phases. *Brazilian Dental Journal* 21: 383–389.

35 Peitl, O., Dutra Zanotto, E., and Hench, L.L. (2001). Highly bioactive P_2O_5–Na_2O–CaO–SiO_2 glass-ceramics. *Journal of Non-Crystalline Solids* 292: 115–126.

36 Peitl, O., La Torre, G.P., and Hench, L.L. (1996). Effect of crystallization on apatite-layer formation of bioactive glass 45S5. *Journal of Biomedical Materials Research* 30: 509–514.

37 Peitl, O., Zanotto, E.D., Serbena, F.C., and Hench, L.L. (2012). Compositional and microstructural design of highly bioactive P_2O_5–Na_2O–CaO–SiO_2 glass-ceramics. *Acta Biomaterialia* 8: 321–332.

38 Daguano, J.K.M.F., Rogero, S.O., Crovace, M.C. et al. (2013). Bioactivity and cytotoxicity of glass and glass-ceramics based on the 3CaO–P_2O_5–SiO_2–MgO system. *Journal of Materials Science: Materials in Medicine* 24: 2171–2180.

39 Vogel, W. and Höland, W. (1987). The development of bioglass ceramics for medical applications. *Angewandte Chemie International Edition in English* 26: 527–544.

40 Vogel, W. and Höland, W. (1990). Development, structure, properties and application of glass-ceramics for medicine. *Journal of Non-Crystalline Solids* 123: 349–353.

41 Höland, W., Wange, P., Naumann, K. et al. (1991). Control of phase formation processes in glass-ceramics for medicine and technology. *Journal of Non-Crystalline Solids* 129: 152–162.

42 Li, H., You, D.Q., Zhou, C.R., and Ran, J.G. (2006). Study on machinable glass-ceramic containing fluorophlogopite for dental CAD/CAM system. *Journal of Materials Science: Materials in Medicine* 17: 1133–1137.

43 Gali, S. (2019). Mica glass ceramics for dental restorations. *Materials and Technology* 34: 2–11.

44 Krüger, S., Deubener, J., Ritzberger, C., and Höland, W. (2013). Nucleation kinetics of lithium metasilicate in ZrO_2-bearing lithium disilicate glasses for dental application. *International Journal of Applied Glass Science* 4: 9–19.

45 Liao, W.-C., Rampf, M., Dittmer, M. et al. (2019). Nucleation and crystal formation in lithium disilicate-apatite glass-ceramic from a combined use of X-ray diffraction, solid-state NMR, and microscopy. *Helvetica Chimica Acta* 102: e1800210.

46 Höland, W., Rheinberger, V., Apel, E., and van't Hoen, C. (2007). Principles and phenomena of bioengineering with glass-ceramics for dental restoration. *Journal of the European Ceramic Society* 27: 1521–1526.

47 Soares, V.O., Serbena, F.C., Mathias, I. et al. (2021). New, tough and strong lithium metasilicate dental glass-ceramic. *Ceramics International* 47: 2793–2801.

48 Höland, W., Rheinberger, V., Wegner, S., and Frank, M. (2000). Needle-like apatite-leucite glass-ceramic as a base material for the veneering of metal restorations in dentistry. *Journal of Materials Science: Materials in Medicine* 11: 11–17.

49 Massera, J. (2020). Bioactive glass-ceramics: from macro to nano. In: *Nanostructured Biomaterials for Regenerative Medicine* (ed. V. Guarino, M. Iafisco and S. Spriano), 275–292. Woodhead Publishing.

50 Gutzow, I., Kashchiev, D., and Avramov, I. (1985). Nucleation and crystallization in glass-forming melts – old problems and new questions. *Journal of Non-Crystalline Solids* 73: 477–499.

51 Schmelzer, J.W.P. (2004). A new approach to nucleation theory and its application to phase formation processes in glass-forming melts. *Physics and Chemistry of Glasses* 45: 116–120.

52 Weinberg, M.C. (1995). Nucleation and crystallization in glass. *Abstracts of Papers of the American Chemical Society* 209: 1–14.

53 Weinberg, M.C. (1999). A few topics concerning nucleation and crystallization in glasses. *Journal of Non-Crystalline Solids* 255: 1–14.

54 Deubener, J., Allix, M., Davis, M.J. et al. (2018). Updated definition of glass-ceramics. *Journal of Non-Crystalline Solids* 501: 3–10.

55 Samuneva, B., Kalimanova, S., Kashchieva, E. et al. (2003). Composite glass-ceramics in the systems $MgO–SiO_2$, $MgO–Al_2O_3–SiO_2$ and fluorapatite obtained by sol–gel technology. *Journal of Sol-Gel Science and Technology* 26: 273–278.

56 Nawaz, Q., de Pablos-Martín, A., e Silva, J.M.S. et al. (2021). Crystallization study of sol–gel derived 13-93 bioactive glass powder. *Journal of the European Ceramic Society* 41 (2): 1695–1706.

57 Nawaz, Q., de Pablos-Martín, A., e Silva, J.M.S. et al. (2020). New insights into the crystallization process of sol–gel-derived 45S5 bioactive glass. *Journal of the American Ceramic Society* 103: 4234–4247.

58 Blaeß, C., Müller, R., Poologasundarampillai, G., and Brauer, D.S. (2019). Sintering and concomitant crystallization of bioactive glasses. *International Journal of Applied Glass Science* 10: 449–462.

59 Yinnon, H. and Uhlmann, D.R. (1982). A kinetic treatment of glass-formation. Transient nucleation in non-isothermal crystallization during cooling. *Journal of Non-Crystalline Solids* 50: 189–202.

60 McMillan, P.W. (1964). *Glass-ceramics*. London/New York: Academic Press.

61 Bocker, C. and Russel, C. (2017). Percolation, phase separation and crystallisation. *Physics and Chemistry of Glasses – European Journal of Glass Science and Technology Part B* 58: 133–141.

62 Deubener, J. (2018). Controlled crystallization of glasses – from transformation kinetics to glass-ceramics. In: *Teaching Glass Better: Tenth Anniversary of the ICG Summer School* (Chapter 11) (ed. A. Takada, J. Parker, A. Duran and K. Bange), 213–231. International Commission on Glass (ICG).

63 Fokin, V.M., Zanotto, E.D., Yuritsyn, N.S., and Schmelzer, J.W.P. (2006). Homogeneous crystal nucleation in silicate glasses: a 40 years perspective. *Journal of Non-Crystalline Solids* 352: 2681–2714.

64 Höland, W., Rheinberger, V., and Frank, M. (1999). Mechanisms of nucleation and controlled crystallization of needle-like apatite in glass-ceramics of the SiO_2–Al_2O_3–K_2O–CaO–P_2O_5 system. *Journal of Non-Crystalline Solids* 253: 170–177.

65 Karpukhina, N., Hill, R.G., and Law, R.V. (2014). Crystallisation in oxide glasses – a tutorial review. *Chemical Society Reviews* 43: 2174–2186.

66 Holand, W., Rheinberger, V., and Schweiger, M. (2003). Control of nucleation in glass ceramics. *Philosophical Transactions of the Royal Society of London, Series A: Mathematical, Physical and Engineering Sciences* 361: 575–588.

67 Krüger, S. and Deubener, J. (2015). Heterogeneous surface nucleation of lithium disilicate glass: an isothermal DSC study. *Journal of Non-Crystalline Solids* 417: 45–51.

68 Cabral, A.A., Fokin, V.M., and Zanotto, E.D. (2004). Nanocrystallization of fresnoite glass. II. Analysis of homogeneous nucleation kinetics. *Journal of Non-Crystalline Solids* 343: 85–90.

69 J.M. Fernández Navarro (2003). *El vidrio, Consejo Superior de Investigaciones Cientificas (CSIC), Madrid*.

70 Fokin, V.M., Yuritsyn, N.S., and Zanotto, E.D. (2005). Nucleation and crystallization kinetics in silicate glasses: theory and experiment. In: *Nucleation Theory and Applications* (ed. J.W.P. Schmelzer), 74–125. Berlin-Weinheim: Wiley-VCH.

71 Krüger, S. and Deubener, J. (2016). The TTT curves of the heterogeneous and homogeneous crystallization of lithium disilicate – a stochastic approach to crystal nucleation. *Frontiers in Materials* 3: 42.

72 Fokin, V.M., Zanotto, E.D., and Schmelzer, J.W.P. (2003). Homogeneous nucleation versus glass transition temperature of silicate glasses. *Journal of Non-Crystalline Solids* 321: 52–65.

73 Macena, G.S., Abyzov, A.S., Fokin, V.M. et al. (2020). Off-stoichiometry effects on crystal nucleation and growth kinetics in soda-lime-silicate glasses. The combeite ($Na_2O{\cdot}2CaO{\cdot}3SiO_2$) – devitrite ($Na_2O{\cdot}3CaO{\cdot}6SiO_2$) joint. *Acta Materialia* 196: 191–199.

74 Zheng, Q.J., Zhang, Y.F., Montazerian, M. et al. (2019). Understanding glass through differential scanning calorimetry. *Chemical Reviews* 119: 7848–7939.

75 Cabral, A.A., Fokin, V.M., Zanotto, E.D., and Chinaglia, C.R. (2003). Nanocrystallization of fresnoite glass. I. Nucleation and growth kinetics. *Journal of Non-Crystalline Solids* 330: 174–186.

76 Zanotto, E.D. (2020). Effect of liquid phase separation on crystal nucleation in glass-formers. Case closed. *Ceramics International* 46: 24779–24791.

77 De Pablos-Martin, A., Patzig, C., Höche, T. et al. (2013). Distribution of thulium in Tm^{3+}-doped oxyfluoride glasses and glass-ceramics. *CrystEngComm* 15: 6979–6985.

78 Höche, T., Patzig, C., Gemming, T. et al. (2012). Temporal evolution of diffusion barriers surrounding $ZrTiO_4$ nuclei in lithia aluminosilicate glass-ceramics. *Crystal Growth and Design* 12: 1556–1563.

79 Kleebusch, E., Rüssel, C., Patzig, C., and Höche, T. (2018). Evidence of epitaxial growth of high-quartz solid solution on $ZrTiO_4$ nuclei in a Li_2O–Al_2O_3–SiO_2 glass. *Journal of Alloys and Compounds* 748: 73–79.

80 Patzig, C., Dittmer, M., Gawronski, A. et al. (2014). Crystallization of ZrO_2-nucleated $MgO/Al_2O_3/SiO_2$ glasses – a TEM study. *CrystEngComm* 16: 6578–6587.

81 Patzig, C., Höche, T., Dittmer, M., and Rüssel, C. (2012). Temporal evolution of crystallization in MgO–Al_2O_3–SiO_2–ZrO_2 glass ceramics. *Crystal Growth and Design* 12: 2059–2067.

82 Vladislavova, L., Thieme, C., Zscheckel, T. et al. (2018). BaO/SrO/ZnO/SiO_2 glass system: influence of different nucleation agents: bulk versus surface crystallisation. In: *NATO Science for Peace and Security Series B: Physics and Biophysics*, 361–366. Dordrecht: Springer.

83 Nascimento, M.L.F. and Zanotto, E.D. (2010). Does viscosity describe the kinetic barrier for crystal growth from the liquidus to the glass transition? *Journal of Chemical Physics* 133: 174701.

84 Cassar, D.R., Rodrigues, A.M., Nascimento, M.L.F., and Zanotto, E.D. (2018). The diffusion coefficient controlling crystal growth in a silicate glass-former. *International Journal of Applied Glass Science* 9: 373–382.

85 de Pablos-Martin, A., Hemono, N., Mather, G.C. et al. (2011). Crystallization kinetics of LaF_3 nanocrystals in an oxyfluoride glass. *Journal of the American Ceramic Society* 94: 2420–2428.

86 Nascimento, M.L.F. and Zanotto, E.D. (2006). Mechanisms and dynamics of crystal growth, viscous flow, and self-diffusion in silica glass. *Physical Review B: Condensed Matter* 73: 024209.

87 Zanotto, E.D. and Cassar, D.R. (2017). The microscopic origin of the extreme glass-forming ability of albite and B_2O_3. *Scientific Reports* 7: 43022.

88 Nascimento, M.L.F., Fokin, V.M., Zanotto, E.D., and Abyzov, A.S. (2011). Dynamic processes in a silicate liquid from above melting to below the glass transition. *Journal of Chemical Physics* 135: 194703.

89 Rodrigues, A.M., Costa, A.M.C., and Cabral, A.A. (2012). Effect of simultaneous nucleation and crystal growth on DSC crystallization peaks of glasses. *Journal of the American Ceramic Society* 95: 2885–2890.

90 Schmelzer, J.W.P., Abyzov, A.S., and Baidakov, V.G. (2017). Time of formation of the first supercritical nucleus, time-lag, and the steady-state nucleation rate. *International Journal of Applied Glass Science* 8: 48–60.

91 Deubener, J., Montazerian, M., Kruger, S. et al. (2017). Heating rate effects in time-dependent homogeneous nucleation in glasses. *Journal of Non-Crystalline Solids* 474: 1–8.

92 Pascual, M., Perez Lara, C., and Duran, A. (2006). Non-isothermal crystallisation kinetics of devitrifying RO–BaO–SiO_2 (R = Mg, Zn) glasses. *Physics and Chemistry of Glasses* 47: 572–581.

93 Pascual, M.J., Durán, A., and Prado, M.O. (2005). A new method for determining fixed viscosity points of glasses. *Physics and Chemistry of Glasses* 46: 512–520.

94 Müller, R., Zanotto, E.D., and Fokin, V.M. (2000). Surface crystallization of silicate glasses: nucleation sites and kinetics. *Journal of Non-Crystalline Solids* 274: 208–231.

95 Höland, W., Rheinberger, V.M., Ritzberger, C., and Apel, E. (2013). Surface or internal nucleation and crystallization of glass-ceramics. *Optical Materials* 35: 1756–1758.

96 Höland, W., Rheinberger, V., and Schweiger, M. (2001). Nucleation and crystallization phenomena in glass-ceramics. *Advanced Engineering Materials* 3: 768–774.

97 Casasola, R., Pérez, J.M., and Romero, M. (2015). Devitrification behavior and preferred crystallization mechanism of glasses based on fluorrichterite ($Na_2CaMg_5Si_8O_{22}F_2$) composition. *Thermochimica Acta* 619: 32–40.

98 Tezvergil-Mutluay, A., Seseogullari-Dirihan, R., Feitosa, V.P. et al. (2017). Effects of composites containing bioactive glasses on demineralized dentin. *Journal of Dental Research* 96: 999–1005.

99 Höland, W., Ritzberger, C., Apel, E. et al. (2008). Formation and crystal growth of needle-like fluoroapatite in functional glass-ceramics. *Journal of Materials Chemistry* 18: 1318–1332.

2

Crystallization of Glasses and Its Impact on Bioactivity and Other Properties

Araceli de Pablos Martín and Delia S. Brauer

Otto Schott Institute of Materials Research, Faculty of Chemistry and Earth Sciences, Friedrich Schiller University, Jena, Germany

2.1 Bioactive Glasses

Bioactive glasses present two main advantages compared to other materials used as clinical bone-grafts [1]: it is possible to tune their physical, chemical, and biological properties via their composition as they do not depend on a specific stoichiometry, and they allow for shaping at elevated temperatures, to obtain fibers, coatings, or complex sintered structures such as three-dimensional porous scaffolds [2]. There are, however, still several open questions, which prevent us from exploiting these materials to their full extent. Many of these questions are related to the crystallization behavior of these glasses and how it affects key properties such as sintering, mechanical stability, and bioactivity. Some researchers claim that this crystallization impedes bioactivity and thus needs to be avoided at all cost [3, 4], while others state that bioactivity is not affected significantly or even improves bioactivity [5–8].

Bioactive glasses contain large amounts of modifier ions (Na^+, K^+, Mg^{2+}, Ca^{2+}), and as a result, their silicate network is highly disrupted, with large concentrations of non-bridging oxygens [9]. This disrupted silicate network is critical for degradation and ion release [10]. However, such a highly disrupted silicate network also means that these glasses crystallize easily during heat treatment, such as sintering [11–13]. This pronounced tendency to crystallize means that a lot of available data on bioactive "glass" scaffolds in the literature actually represent data on glass-ceramics or crystallized glasses [14].

The design of bioactive glasses is often based on the network connectivity (NC) model. NC is the average number of bridging oxygens per network forming element (here silicon) in the glass structure [9, 15]. Considering a maximum of four bridging oxygen atoms per silicon atom, and phosphorus only present as orthophosphate species (PO_4^{3-}) [9], NC of a glass is calculated according to Eq. (2.1), where $M^I{}_2O$ and $M^{II}O$ are typical modifier oxides [16, 17]:

$$NC_{Si} = \frac{4\left[SiO_2\right] - 2\left[M^I{}_2O + M^{II}O\right] + 6\left[P_2O_5\right]}{\left[SiO_2\right]} \tag{2.1}$$

NC must be adjusted to fulfill the ion release requirements and thus, the bioactivity, while maintaining the desired thermal behavior and stability, e.g. tendency to crystallize. An NC between 2.0 and 2.6 has been suggested optimum for bioactive glasses [18], and while NC = 2.4 has been put forward as the cutoff value for bioactivity [19], glasses with higher NC have been shown to degrade and surface mineralize in aqueous environments and perform well during *in vitro* cell culture studies [20].

Bioactive Glasses and Glass-Ceramics: Fundamentals and Applications, First Edition.
Edited by Francesco Baino and Saeid Kargozar.

2.2 Bioactive Glass-Ceramics

Glass-ceramics are prepared by controlled crystallization of glasses. Initially, the motivation to study bioactive glass-ceramics originated from the mechanical limitations of bioactive glasses [21]. Results indicated, though, that additional improvements can be obtained by crystallization. In 1982, Kokubo et al. [22] developed the bioactive glass-ceramic Cerabone-AW® (Nippon Electric Glass Co, Japan), obtained from the crystallization of a glass in the system SiO_2–P_2O_5–CaO–MgO–CaF_2, containing oxyfluorapatite and wollastonite crystal phases. This glass-ceramic not only exhibits much better mechanical properties than bioactive glasses, it also forms a tight bond to bone *in vivo*. Moreover, it can be machined into various shapes, which is an important benefit for clinical applications [22–24]. Since then, glass-ceramics have been used clinically as structural materials in load-bearing applications such as vertebral spacers or iliac crest prostheses [25].

Beside the possibility to tune properties via composition, glass-ceramics provide an additional variable with the type of crystalline phase(s) present. The presence of certain crystalline phases can be tuned via glass composition and subsequent heat treatment. As shown below, the nature of the crystals embedded in the glassy matrix as well as their morphology, size, and quantity has tremendous influence on the thermal, mechanical, and biological properties of a glass-ceramic. On the one hand, the mechanical properties of glass-ceramics are superior than those of glasses [26, 27]; on the other hand, crystallization may compromise bioactivity in some cases. Thus, to achieve an ideal biomaterial, a balance between bioactivity and mechanical strength must be achieved.

2.3 Influence of Crystallization on Processing

The thermal properties of a glass determine the processing regime for bioactive glasses and glass-ceramics, while thermal properties in turn are governed by glass composition and structure. Controlled crystallization is key for tailoring the properties of glass-ceramics. Spontaneous crystallization, by contrast, caused by a pronounced tendency to devitrify during cooling of the melt, is undesirable because it prevents us from obtaining a bioactive glass in an amorphous state and makes it challenging if not impossible to control crystal phases, number, and size via heat treatment.

There are two main network formers in bioactive glasses: SiO_2 and P_2O_5. In general, it can be said that SiO_2 provides a low-solubility matrix that compensates the excess of solubility of the phosphate part. The role of network formers in the structure of bioactive glasses and glass-ceramics, their crystallization and bioactivity have been discussed previously [9, 15, 28, 29]. In general, while SiO_2 increases glass stability against crystallization, P_2O_5 can favor crystallization through phase separation, or strongly reduce the nucleation rate above a threshold content [28].

Bioactive glasses tend to crystallize easily during both cooling of the melt and heat treatment of a glass, and one main reason is their low NC compared to conventional silicate glasses. This low degree of polymerization of the silicate network causes a high mobility of network fragments at high temperatures, thus facilitating nucleation and subsequent crystallization. While many bioactive glasses show surface crystallization (Figure 2.1), one of the most well-known compositions, Bioglass 45S5, shows both surface and internal crystallization [33], which seems to impede viscous flow for both bulk (Figure 2.1a,b) and powder samples (Figure 2.1c,f) [31, 34, 35], thereby impeding full densification [21]. Only when physical load is applied during sintering, densely sintered

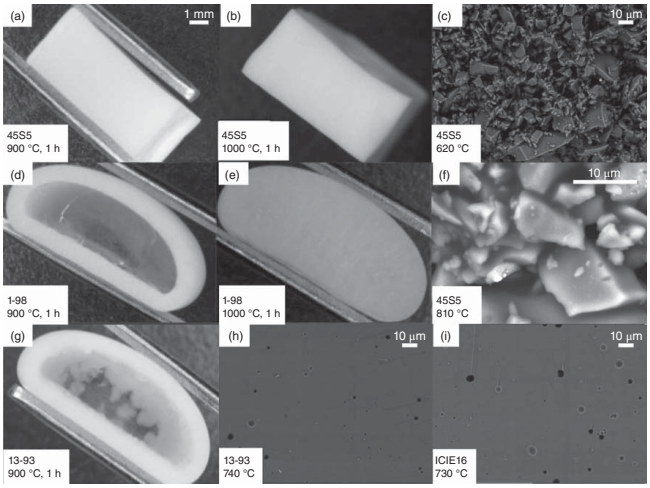

Figure 2.1 Cross sections of heat-treated bioactive glass bulk pieces (a, b) 45S5, (d, e) 1-98, and (g) 13-93 and of heat-treated powder compacts (c, f) 45S5, (h) 13-93, and (i) ICIE16. Compositions (d, e) 1-98 and (g) 13-93 started to flow during heat treatment, causing their shape to become rounded. By contrast (a, b) 45S5 kept the cubic shape. In addition, during sintering of (c, f) 45S5 powder at temperatures up to 300 K above glass transition, no dense sintering occurred and individual grains can still be distinguished, while during the sintering of powders of (h) 13-93 or (i) ICIE16 only small round pores remained behind. Source: (a, b, d, e) Arstila et al. [30], Figure 01, p. 03/with permission of Elsevier; (c, f, h, i) Blaeß et al. [31], Figure 02, p. 05/John Wiley & Sons, Inc./CC BY 4.0; (g) Fagerlund et al. [32], Figure 03, p. 04/with permission of Elsevier.

Bioglass 45S5 powder compacts can be obtained [34]. To facilitate the sintering of porous scaffolds without crystallization occurring, several bioactive glasses with a reduced crystallization tendency have been developed, e.g. 13-93 (Figure 2.1g,h [36]) or ICIE1 (Figure 2.1i [37]). Crystallization does not always negatively affect sintering; however, key is that the crystal phases forming do not impede viscous flow sintering [31].

In order to obtain glass-ceramics of a desired shape, processing is necessary. Systems which crystallize by a volume nucleation process, i.e. showing internal crystallization, can be cast to shape from the melt. The resulting glass is then exposed to an additional heat-treatment procedure where crystallization is achieved. Apatite-mullite glass-ceramics are a good example for such a system [24]. By contrast, in Kokubo's apatite-wollastonite glass-ceramic [22], both crystal phases formed by surface crystallization, and heat treatment of the bulk glass is not a viable option to obtain mechanically stable bulk glass-ceramic pieces. Implants are therefore prepared by heat treating powder compacts to allow for shaping while still having a homogeneous distribution of crystals distributed in the bulk and obtaining good mechanical stability.

2.4 Influence of Crystallization on Mechanical Properties

The mechanical properties of implants need to be suited to the application of the material. First, the morphology of the bioactive glass-ceramics must be considered. Whether the final product is intended to be used as powder, granules, slurries or scaffolds, or as monoliths, to be machined to specific geometries, is crucial to determine the mechanical properties needed. Second, an estimate of the mechanical stresses, to which the material is exposed, is also needed, as the load impact of a knee or a tooth prothesis is not the same as that of a middle-ear implant. For this reason, Bioglass 45S5 bulk pieces were used successfully as implants to replace the ossicular chain in the middle ear [3] as mechanical load here is negligible and the mechanical properties of Bioglass were acceptable. Another example is the glass-ceramic Ceravital, which was also used as middle-ear implants [27], despite its mechanical properties being below the 160 MPa of the human cortical bone. (It later turned out, however, that fast degradation of Ceravital prevented its successful use as ossicular prostheses [38].)

It is well known that the mechanical properties of glass-ceramics are superior of those of glasses [26, 27]. The presence of crystals embedded in a glassy matrix is responsible for crack deflections and, thus, for improving the resistance to crack propagation. If crystallization of glass powders (e.g. during the preparation of scaffolds) occurs at lower temperatures than the end of the sintering, however, full densification is not achieved (Figure 2.1c,f) and the mechanical properties may be compromised [31, 34, 35]. As a result, mechanical stability of sintered constructs such as porous scaffolds tends to be lower for 45S5 than for bioactive glasses with improved sintering such as 13-93 [22]. By contrast, if crystallization takes place in a controlled manner, not only the mechanical properties but also the bioactivity can be improved with respect to those of the parent glasses. Thus, where crystallization originally seemed to be a disadvantage, it has become a possibility to improve these materials, by turning glasses into glass-ceramics.

Studies on Biosilicate [39] showed that the glass-ceramic with 34% of crystalline volume showed much better mechanical properties than the parent glass, while the crystal size seemed to have a lower influence on mechanical performance. The type of crystal phases present can also have direct influence on the mechanical properties of a glass-ceramic. This is particularly noticeable in apatite-containing glass-ceramics such as the apatite-wollastonie, apatite-mica, or apatite-mullite systems [24], where the function of the apatite phase was to provide bioactivity (as

discussed below), while the additional phase provided mechanical strength. The glass-ceramic Cerabone-AW possesses excellent mechanical properties [24, 27, 40]. Of the crystalline phases present, wollastonite ($CaSiO_3$) strongly improves the mechanical properties of glass-ceramics. Especially compressive strength (up to 1080 MPa), flexural strength (up to 215 MPa), Young's modulus (118 GPa), and fracture toughness (up to 2 $MPa/m^{1/2}$) are much higher than those of bioactive glass-ceramics without wollastonite crystal phase [24]. Machinability of glass-ceramics is important in orthopedics and dentistry. In the Bioverit glass-ceramics, machinability originates from the presence of mica crystals. While both Bioverit I and Bioverit II contain a mica crystal phase, the mica crystals present in Bioverit I show the typical morphology of flat flakes, while those present in Bioverit II are curved, arranging themselves in spherical lamellae, giving the crystals a cabbage-like appearance [41, 42]. As a result, Bioverit II is easier to machine than Bioverit I. The influence of variation in composition or heat treatment on glass-ceramic microstructure is illustrated in Figure 2.2, using Bioverit as an example [41, 43, 44, 47].

2.5 Influence of Crystallization on Bioactivity

In the literature, the term "bioactivity" of glasses or glass-ceramics may refer to one of several aspects of behavior. Strictly speaking, bioactivity can only be tested *in vivo*, showing the integration of an implant material into the living tissue, such as the bonding of bioactive glasses to bone [48]. Many people, however, refer to *in vitro* apatite formation as "bioactivity," even if no living system, not even cells *in vitro*, are present. Others talk about bioactivity if compositions have shown good results during *in vitro* cell culture studies, e.g. with osteoblasts or other relevant cell lines. In this chapter, to avoid confusion, we will refer to "*in vitro* apatite formation" when talking about the precipitation of apatite-like crystal phases on the surface of a bioactive glass or glass-ceramic when immersed in acellular simulated physiological solutions (such as simulated body fluid, SBF). When referring to results from cell culture studies, we will talk about "*in vitro* bioactivity."

Bioactivity *in vitro* or *in vivo* is often related to solubility or ion release rate from a material. In addition, for many bioactive glasses or glass-ceramics, the subsequent process of surface mineralization, e.g. by apatite precipitation, plays a significant role. Both differ for glasses and glass-ceramics, and for the latter, they also vary with composition of the crystalline phase, as shown in Table 2.1.

We will first look at the effect of **solubility** or ion release. It has long been known that bioactive glasses not only bond to living tissue when implanted but they also degrade over time [53, 54], allowing for bone to be regenerated and, eventually, replaced by the body's own bone tissue [55]. Degradation rate here needs to match the rate of tissue formation. If the implant degrades too fast, not only will this prevent cells from attaching and proliferating on the implant surface but also high ionic concentrations owing to fast dissolution may compromise cell viability and result in cytotoxicity [56]. While the pronounced pH increase caused by fast ion release from Bioglass 45S5 makes preconditioning necessary for *in vitro* cell culture studies [57], this has not prevented its successful clinical application [58], showing that *in vivo* fluid exchange may overcome some issues related to degradation and solubility. The inherent release of ions from bioactive glasses is also related to their bioactivity *in vitro* and *in vivo*. The controlled release of ions in therapeutic concentrations, e.g. the release of specific amounts of soluble silica species, has been shown to stimulate cells *in vitro* [59], making bioactive glasses of interest for the controlled release of therapeutic ions directly at the implant site [60]. In addition, the release of ions such as calcium or phosphate is a key step during the formation of mineralized surface layers, as discussed further below.

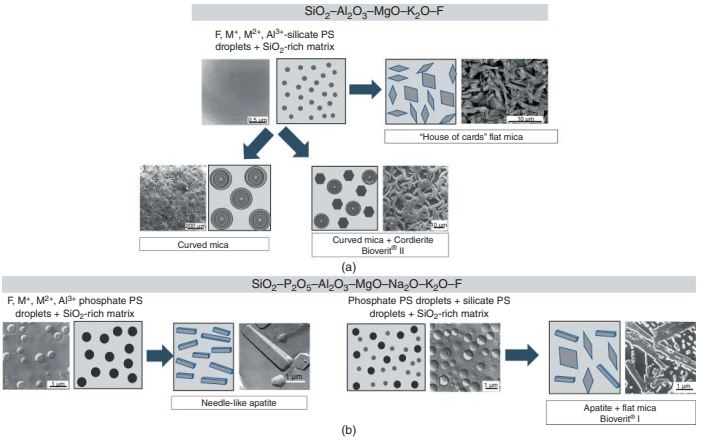

Figure 2.2 Influence of changes in composition or heat treatment regime on crystal type (phlogopite mica, apatite) and microstructures of Bioverit glass-ceramics [41, 43, 44]. Arrows indicate heat treatment. (a) $SiO_2–Al_2O_3–MgO–K_2O–F$ system. The base glass shows silicate phase separation (PS) droplets. Controlled crystallization resulted in flat, flake-shaped ("house of cards") phlogopite mica $Na/KMg_3AlSi_3O_{10}F_2$. After increasing the Al_2O_3 and MgO content, curved phlogopite mica crystallized. As the glassy matrix becomes depleted in F and alkali during mica crystallization, additional crystallization of cordierite, $Mg_2(Si_5Al_4O_{18})$, takes place (the same thing happens if the concentrations of MgO and Al_2O_3 increase further with respect to SiO_2), which is the final microstructure of Bioverit II. By controlling both crystallizations, it is possible to tune the degree of transparency of the final glass-ceramic. (b) An increase in CaO and P_2O_5 content can lead to the separation in two or three phases (left and right, respectively). (b, left) In the P_2O_5-enriched mica-based glass-ceramic-controlled heat treatment leads to crystallization of needle-like apatite. (b, right) For high MgO and Al_2O_3 content in addition to P_2O_5 enrichment, three phases are formed in the glass. From the small droplet phase rich in Si, M^+, and F, flat mica crystals form, while the large droplet phase rich in M^{2+}, P_2O_5, and F leads to homogeneous nucleation of apatite, resulting in the typical microstructure of Bioverit I. Source: Micrographs of silicate PS droplets, curved mica, and phosphate PS droplets adapted with permission from Vogel et al. [44], Figure 03, 07, 08, p 04, 07, 08 / With permission of Elsevier. Micrograph of the house-of-cards flat mica reprinted with permission from Rashwan et al. [45], Figure 05, p 06 / With permission of Elsevier. Micrographs of curved mica and cordierite, phosphate and silicate PS droplets and apatite-flat mica reprinted with permission from Vogel and Höland [43], Figure 01, 02, 03, p 02, 03 / With permission of Elsevier. Micrograph of apatite needles reprinted with permission from Höche et al. [46], Figure 03, p 05 / With permission of American Chemical Society.

A crystalline phase is more thermodynamically stable than an amorphous phase of the same composition, providing bioactive glasses with a higher solubility than the respective crystalline materials. Controlled crystallization thus reduces and can even tune the dissolution rate, enabling a better control of cytotoxicity [51]. For some phosphate glass compositions, an increased solubility of the glass-ceramic compared to the parent glass has been reported [61], showing that it is not the presence or absence of crystalline phases *per se* but the type of crystal phase which needs to be considered. Some studies pointed out that volume crystallization leads to a lower cytotoxicity than surface crystallization [52]. Silicon ion release was reported not to vary significantly with crystallization [23], which may be related more to the low solubility of silica species in aqueous solutions [62]. In each case, however, solubility of the final glass-ceramics not only depends on the type and relative amount of crystal phases present but also on the composition and structure of the glassy matrix. If the NC of the glassy matrix in a glass-ceramic is higher than that of the parent glass, it can be expected to have a lower solubility. Should the NC of the glassy matrix remain constant, however, solubility can be expected not to change.

The mechanism of interaction between a 45S5-based glass-ceramic surface and SBF was shown to comprise the following stages [35]: (i) preferential dissolution at glass/crystal interfaces, (ii) preferential dissolution at crystal structural defects causing break-down of crystalline particles into finer grains, and (iii) amorphization through introduction of point defects produced during ion exchange, leading to an optimum ion release in the studied glass-ceramics. Therefore, the assumption that ion release decreases with decreasing residual glassy matrix must be considered carefully.

The second factor affecting bioactivity is surface **apatite formation** in contact with physiological solutions. It is typically lower for crystalline solids than for amorphous glasses [63], likely owing to lower ion release from crystalline phases. Li et al. [4] suggested that apatite deposition on the surface of a bioactive glass is caused by the formation of a negatively charged surface, which attracts cations (Ca^{2+}) from the solution. Such a negatively charged surface is formed when cationic species, i.e. modifier ions, are released from the glass. According to them, the existence of a residual glassy matrix is key for the deposition of an apatite layer on the surface of the glass-ceramics.

However, other studies reported on crystallization not inhibiting the development of an apatite surface layer, even in fully crystallized glass-ceramics, although the kinetics differed for glasses and glass-ceramics. Peitl et al. [49] studied apatite formation on 45S5 glass-ceramics during immersion in SBF. They reported that while all glass-ceramics, with crystallinity ranging from 8% to 100%, formed an apatite surface layer during immersion, the onset of apatite formation shifted from 10 hours for the amorphous glass to 22–25 hours for the 60–100% crystalline material.

The formation of a crystalline apatite layer depends on several variables, including the rate of ion exchange, hydroxylation of the glass surface, and pH and ion concentration of the solution. The effect of crystallinity on apatite formation appears to be related to the connectivity of the residual glassy phase, which controls the rate of ion exchange and silanol formation. The generally observed trend is that the crystallization of silicate phases delays but not inhibits the formation of the apatite layer [64–66] with respect to the parent glasses (Table 2.1). Many bioactive glass-ceramics contain a phosphate crystal phase, typically an apatite phase either on its own or together with silicate crystal phases. Duminis et al. [24] and Chen et al. [29] postulate that apatite crystals within a glass-ceramic may act as nuclei for apatite surface precipitation, by reducing the apatite nucleation energy, which is typically the limiting factor of apatite crystallization. It further has been reported that apatite surface precipitation was five times faster in a whitlockite (calcium phosphate phase) glass-ceramic than in the precursor glass [51]. The authors explained this with two characteristics of the crystalline phase whitlockite: it is a soluble phase, and it accelerates the crystallization of hydroxycarbonate apatite (HCA) by acting as a preferential site for nucleation and crystal growth.

Table 2.1 Selection of bioactive glass-ceramics reported in literature and comparison of the ***in vitro* bioactivity** between glasses and glass-ceramics.

Glass composition (wt%)	Crystalline phase (heat treatment)	Crystallinity	Test solution	*In vitro* bioactive properties of the glass(es)	*In vitro* bioactive properties of the GCs	References
$48SiO_2$ $9.5P_2O_5$ $20Na_2O$ 22.5CaO	$Na_2CaSi_3O_8$ $Ca_{10}(PO_4)_6(O(OH)_2)$ (nucleation at 670 °C – 15–180 min; crystallization at 750 °C – 15–180 min)	62–100%	Tris buffer	HCA formation within 5 h	HCA layer formed in GC with 62% and 89% crystalline fraction after >100 h immersion No HCA formation in GCs from 95% crystal phase	Li et al. [4]
Bioglass 45S5 $45SiO_2$ $6P_2O_5$ $24.5Na_2O$ 24.5CaO	$Na_2Ca_2Si_3O_9$ (nucleation at 550 °C – 150 h; crystallization at 680 °C – 113–66 min)	8–100 vol%	SBF	HCA formation after 8 h	No inhibition of HCA formation even with a fully crystallized GC Onset of HCA crystallization increases with crystallinity up to 22–25 h for the 60–100% crystalline material	Peitl et al. [49]
$47.5–50.3SiO_2$ $23.2–18.5Na_2O$ 23.2–31.3CaO $0–6P_2O_5$	$Na_2Ca_2Si_3O_9$ (nucleation at 520–590 °C – 3 min to 150 h; crystallization at 620–700 °C – 5–80 min)	5–100%	SBF	Onset of HCA formation increases with decreasing P content between 8 h (6% P_2O_5) and 31 h (0% P_2O_5)	Onset of HCA crystallization increases with crystallinity between 12 h (10% crystallinity) and 25 h (100% crystallinity), and decreases with the addition of P_2O_5	Peitl et al. [7]

Table 2.1 (Continued)

Glass composition (wt%)	Crystalline phase (heat treatment)	Crystallinity	Test solution	*In vitro* bioactive properties of the glass(es)	*In vitro* bioactive properties of the GCs	References
Bioglass 45S5 47.3SiO_2 22.1Na_2O 24.2CaO (after chemical analysis) 6.2P_2O_5	$Na_2Ca_2Si_3O_9$ (1000 °C – 1 h)	100%	SBF (large SBF volume/glass surface ratio)	Ca_2SiO_4 layer formed on the surface after 7 d, $CaCO_3$ layer after 14 d immersion No apatite formation (aggressive corrosion under the SBF test conditions)	Apatite formation after 7 and 14 d immersion	Plewinski et al. [50]
(mol%) 28.4–38.1SiO_2 41.4–55.5CaO/SrO 4.7–6.3P_2O_5 0–25.5CaF_2/SrF_2	Compositions with high CaF_2/SrF_2 content: uncontrolled crystallization of FAp and CaF_2/SrF_2 upon cooling of the melt	n.m.	SBF, Tris buffer	FAp formation within 3 h in Tris and within 24 h in SBF P release: very small percentages (less than 2%)	FAp formation between 3 and 6 h in both, Tris and SBF Precrystallization favors further FAp formation during immersion P release: higher concentrations (up to 11%)	Chen et al. [29]
52.75$Ca_3(PO_4)_2$ 30SiO_2 17.25MgO	3(Ca,Mg)O·P_2O_5 (775 °C–4h) 3(Ca,Mg)O·P_2O_5 + not cataloged silicate (775 and 975 °C–4h)	27% 63%	SBF	Formation of an amorphous Ca–P layer after 48 h Onset of HCA formation after 5 d	GC-27% crystallinity: onset for HCA formation after 24 h and complete formation after 7 d Data nonconclusive for the GC-63% crystallinity	Daguano et al. [51]
(in mol%) 75$NaPO_3$–(25 − x) CaO–xCaF_2 (x = 0, 5, 10, 15, 20)	$Ca_2P_2O_7$ CaF_2 for x = 20	n.m.	Tris buffer	An increase in CaF_2 content leads to an increase in glass solubility	The high dissolution rate of the CaF_2-free (x = 0) GC leads to the loss of bioactivity and increased cytotoxicity. The GC with x = 20 shows bioactivity and a faster dissolution compared to the glass when immersed for up to 6 h in Tris buffer, but it shows slower dissolution than the glass at longer immersion times	Nommeots-Nomm et al. [52]

GC, glass-ceramic; SBF, simulated body fluid; HCA, hydroxycarbonate apatite; FAp, fluorapatite; TCP, $Ca_3(PO_4)_2$; W, $CaSiO_3$; T, 3MgO·4SiO_2; n.m., not mentioned.

Glass-ceramics in which phosphate phases or both silicate and phosphate phases crystallize have been studied extensively [24, 67–71]. Besides apatite, crystalline phases include rhenanite [72] and various calcium phosphates [52, 73].

Factors mentioned above may also to some extent affect bioactivity *in vitro* and *in vivo*. Azenha et al. [74] report on two similar glass-ceramics in the system SiO_2–CaO–MgO–P_2O_5–Al_2O_3–F, both containing apatite and wollastonite crystal phases in similar weight percentages but showing completely different bioactivity. While the glass-ceramic with higher Al_2O_3 content (19.04 mol%) in the residual glassy matrix was bioinert, the glass with much lower content (1.19 mol%) showed bioactivity *in vitro* and *in vivo*. Thus, not only the NC of the parent glass should be considered, but in the case of glass-ceramics also that of the residual glassy matrix.

Unlike glasses, glass-ceramics present a nonhomogeneous elemental distribution, owing to elemental depletions and enrichments caused by the formation of crystalline phases [74]. Living cells are pH sensitive, and *in vitro* cell culture experiments have shown cells reacting positively to the presence of Na-enriched areas in a glass-ceramic, which produced a slightly alkaline pH favorable to osteoblast differentiation and function. This means that this nonhomogenous microstructure facilitated a beneficial release of ions here in a way more effective than in an amorphous material with homogeneous elemental distribution [75].

Kokubo's apatite-wollastonite (Cerabone) glass-ceramics show a high bioactivity *in vivo*, with bonding to bone apparently occurring via the formation of a calcium phosphate surface layer bearing pronounced similarity to apatite [76]. This bond to bone has been shown to be so strong that tensile fracture never occurs at the glass-ceramic/bone interface, but rather in the bone [23]. Interestingly, apatite-wollastonite glass-ceramics did not form such an apatite-like surface layer during immersion experiments in Tris buffer solution *in vitro*, inspiring Kokubo to develop his SBF [77].

In vivo studies [78] have suggested that the presence of an apatite crystal phase within a glass-ceramic induces bone bonding in an otherwise bioinert material. Here, a glass of the composition $4.5SiO_2$–$3Al_2O_3$–$3.2P_2O_5$–3CaO–$1.51CaF_2$ (mol%) was either implanted into rat femurs as-cast, i.e. in a glassy state, or heat-treated before implantation to obtain a glass-ceramic containing principally fluorapatite or both fluorapatite and mullite as crystal phases. While the amorphous glass showed no integration with bone at four weeks, both glass-ceramics showed good integration with intimate bone contact.

We take this as an indication that the presence of apatite crystals, whether by crystallization following heat treatment or by surface mineralization creates a biomimetic environment, which bone cells adhere to, proliferate and differentiate on to form bone. Depending on the nature and extent of additional processes such as ion release or degradation, this bone integration may be further enhanced or slowed down.

2.6 Conclusions and Perspectives

Spontaneous, i.e. uncontrolled, crystallization of bioactive glasses is well known to negatively affect performance. This is particularly noticeable for Bioglass 45S5, where crystallization impedes viscous flow sintering and thereby drastically lowers the mechanical properties of scaffolds. Crystallization of the silicate network slows down degradation, ion release, and apatite surface precipitation, but several materials containing such phases, e.g. Biosilicate or Cerabone (apatite-wollastonite) glass-ceramics, have shown that this does not necessarily translate to lower *in vivo* bioactivity. Controlled crystallization is an excellent tool for fine-tuning of various materials properties. Especially the crystallization of apatite-type phases may induce bioactivity

to otherwise inert materials. But controlled crystallization is particularly useful to improve mechanical properties, with glass-ceramics currently used in dental restorations (see Chapter 18) showing excellent strength. While bioactive glasses, e.g. compositions Bioglass 45S5 or BonAlive S53P4, have been used successfully as bone regeneration materials, their glassy nature limits their use to nonload bearing applications. Nevertheless, one focus in bioactive glass research has long been to avoid crystallization during sintering. Depending on the effect of crystallization on type, size, and morphology of crystals forming as well as on the properties of the glassy matrix; however, changes in properties may actually be favorable rather than destructive.

We hope that reading this chapter encourages researchers in the field of bioactive glasses to embrace controlled crystallization as a valuable tool for tailoring the properties of bioactive glasses in order to broaden their application range and pave the way toward new clinical implant materials.

References

1 Gong, T., Xie, J., Liao, J. et al. (2015). Nanomaterials and bone regeneration. *Bone Research* 3: 15029.

2 Jones, J. (2009). New trends in bioactive scaffolds: the importance of nanostructure. *Journal of the European Ceramic Society* 29: 1275–1281.

3 Jones, J.R. (2013). Review of bioactive glass: from Hench to hybrids. *Acta Biomaterialia* 9: 4457–4486.

4 Li, P., Yang, Q., Zhang, F., and Kokubo, T. (1992). The effect of residual glassy phase in a bioactive glass-ceramic on the formation of its surface apatite layer in vitro. *Journal of Materials Science – Materials in Medicine* 3: 452–456.

5 Al-Noaman, A., Rawlinson, S.C.F., and Hill, R.G. (2012). The role of MgO on thermal properties, structure and bioactivity of bioactive glass coating for dental implants. *Journal of Non-Crystalline Solids* 358: 3019–3027.

6 Magallanes-Perdomo, M., Luklinska, Z.B., De Aza, A.H. et al. (2011). Bone-like forming ability of apatite–wollastonite glass ceramic. *Journal of the European Ceramic Society* 31: 1549–1561.

7 Peitl, O., Dutra Zanotto, E., and Hench, L.L. (2001). Highly bioactive P_2O_5–Na_2O–CaO–SiO_2 glass-ceramics. *Journal of Non-Crystalline Solids* 292: 115–126.

8 Peitl, O., Zanotto, E.D., Serbena, F.C., and Hench, L.L. (2013). Bioactive glass-ceramics for load-bearing applications. In: *An Introduction to Bioceramics*, Default Book Series, 2e (ed. L.L. Hench), 495–503.

9 Brauer, D.S. (2015). Bioactive glasses – structure and properties. *Angewandte Chemie International Edition* 54: 4160–4181.

10 Tilocca, A. and Cormack, A.N. (2008). Exploring the surface of bioactive glasses: water adsorption and reactivity. *Journal of Physical Chemistry C* 112: 11936–11945.

11 Cengiz, I.F., Oliveira, J.M., and Reis, R.L. (2018). Micro-CT – a digital 3D microstructural voyage into scaffolds: a systematic review of the reported methods and results. *Biomaterials Research* 22: 26.

12 Negut, I., Dorcioman, G., and Grumezescu, V. (2020). Scaffolds for wound healing applications. *Polymers* 12: 1–19.

13 Qu, H., Han, Z., Zhuo, Y., and Fu, H. (2019). Review of the design of porous bio-scaffolds for bone tissue engineering. *Journal of Mechanical Engineering* 55: 71–80.

14 Chen, Q.Z., Thompson, I.D., and Boccaccini, A.R. (2006). 45S5 Bioglass®-derived glass-ceramic scaffolds for bone tissue engineering. *Biomaterials* 27: 2414–2425.

15 Hill, R.G. and Brauer, D.S. (2011). Predicting the bioactivity of glasses using the network connectivity or split network models. *Journal of Non-Crystalline Solids* 357: 3884–3887.

16 Dietzel, A. (1941). Strukturchemie des Glases. *Naturwissenschaften* 29: 537–547.

17 Dietzel, A. (1942). Die Kationenfeldstärken und ihre Beziehungen zu Entglasungsvorgängen, zur Verbindungsbildung und zu den Schmelzpunkten von Silicaten. *Zeitschrift für Elektrochemie* 48: 9–23.

18 Eden, M., Sundberg, P., and Stalhandske, C. (2011). The split network analysis for exploring composition–structure correlations in multi-component glasses: II. Multinuclear NMR studies of alumino-borosilicates and glass-wool fibers. *Journal of Non-Crystalline Solids* 357: 1587–1594.

19 Hill, R. (1996). An alternative view of the degradation of bioglass. *Journal of Materials Science Letters* 15: 1122–1125.

20 Hoppe, A., Jokic, B., Janackovic, D. et al. (2014). Cobalt-releasing 1393 bioactive glass-derived scaffolds for bone tissue engineering applications. *ACS Applied Materials & Interfaces* 6: 2865–2877.

21 Montazerian, M. and Zanotto, E.D. (2016). History and trends of bioactive glass-ceramics. *Journal of Biomedical Materials Research Part A* 104: 1231–1249.

22 Kokubo, T., Shigematsu, M., Nagashima, Y. et al. (1982). Apatite- and wollastonite-containing glass-ceramics for prosthetic application. *Bulletin of the Institute for Chemical Research, Kyoto University* 60: 260–268.

23 Kokubo, T. (1991). Bioactive glass ceramics: properties and applications. *Biomaterials* 12: 155–163.

24 Duminis, T., Shahid, S., and Hill, R.G. (2017). Apatite glass-ceramics: a review. *Frontiers in Materials Research* 3: 1–15.

25 Hench, L.L. (1998). Bioceramics. *Journal of the American Ceramic Society* 81: 1705–1728.

26 Höland, W. and Beall, G.H. (2012). *Glass-Ceramic Technology*. Wiley.

27 de Aza Moya, A.H., de Aza Pendas, S., De Aza, P.N., and Pena, P. (2007). Bioactive glasses and glass-ceramics. *Boletín de la Sociedad Española de Cerámica y Vidrio* 46: 45–55.

28 Brauer, D.S. and Möncke, D. (2017). Introduction to the structure of silicate, phosphate and borate glasses. In: *Bioactive Glasses: Fundamentals, Technology and Applications, RSC Smart Materials* (Chapter 3) (ed. A.R. Boccaccini, D.S. Brauer and L. Hupa), 61–88. RSC.

29 Chen, X., Chen, X., Brauer, D.S. et al. (2014). Bioactivity of sodium free fluoride containing glasses and glass-ceramics. *Materials* 7: 5470–5487.

30 Arstila, H., Hupa, L., Karlsson, K.H., and Hupa, M. (2008). Influence of heat treatment on crystallization of bioactive glasses. *Journal of Non-Crystalline Solids* 354: 722–728.

31 Blaeß, C., Müller, R., Poologasundarampillai, G., and Brauer, D.S. (2019). Sintering and concomitant crystallization of bioactive glasses. *International Journal of Applied Glass Science* 10: 449–462.

32 Fagerlund, S., Massera, J., Hupa, M., and Hupa, L. (2012). T-T-T behaviour of bioactive glasses 1-98 and 13-93. *Journal of the European Ceramic Society* 32: 2731–2738.

33 Massera, J., Fagerlund, S., Hupa, L., and Hupa, M. (2012). Crystallization mechanism of the bioactive glasses, 45S5 and S53P4. *Journal of the American Ceramic Society* 95: 607–613.

34 Guillon, O., Cao, S., Chang, J. et al. (2011). Effect of uniaxial load on the sintering behaviour of 45S5 Bioglass® powder compacts. *Journal of the European Ceramic Society* 31: 999–1007.

35 Boccaccini, A.R., Chen, Q., Lefebvre, L. et al. (2007). Sintering, crystallisation and biodegradation behaviour of Bioglass®-derived glass-ceramics. *Faraday Discussions* 136: 27–44.

36 Brink, M. (1997). The influence of alkali and alkaline earths on the working range for bioactive glasses. *Journal of Biomedical Materials Research* 36: 109–117.

37 Elgayar, I., Aliev, A.E., Boccaccini, A.R., and Hill, R.G. (2005). Structural analysis of bioactive glasses. *Journal of Non-Crystalline Solids* 351: 173–183.

38 Brewis, C., Orrell, J., and Yung, M.W. (2003). Ceravital revisited: lessons to be learned. *Otology & Neurotology* 24: 20–23.

39 Peitl, O., Zanotto, E.D., Serbena, F.C., and Hench, L.L. (2012). Compositional and microstructural design of highly bioactive P_2O_5–Na_2O–CaO–SiO_2 glass-ceramics. *Acta Biomaterialia* 8: 321–332.

40 Crovace, M.C., Souza, M.T., Chinaglia, C.R. et al. (2016). Biosilicate® – a multipurpose, highly bioactive glass-ceramic. In vitro, in vivo and clinical trials. *Journal of Non-Crystalline Solids* 432: 90–110.

41 Vogel, W. and Höland, W. (1987). The development of bioglass ceramics for medical applications. *Angewandte Chemie International Edition in English* 26: 527–544.

42 Gebhardt, A., Höche, T., Carl, G., and Khodos, I.I. (1999). TEM study on the origin of cabbage-shaped mica crystal aggregates in machinable glass-ceramics. *Acta Materialia* 47: 4427–4434.

43 Vogel, W. and Höland, W. (1990). Development, structure, properties and application of glass-ceramics for medicine. *Journal of Non-Crystalline Solids* 123: 349–353.

44 Vogel, W., Höland, W., Naumann, K., and Gummel, J. (1986). Development of machineable bioactive glass ceramics for medical uses. *Journal of Non-Crystalline Solids* 80: 34–51.

45 Rashwan, M., Cattell, M., and Hill, R. (2019). The effect of barium content on the crystallization and microhardness of barium fluormica glass-ceramics. *Journal of the European Ceramic Society* 39: 2559–2565.

46 Höche, T., Moisescu, C., Avramov, I. et al. (2001). Microstructure of SiO_2–Al_2O_3–CaO–P_2O_5–K_2O–F^- glass ceramics. 1. Needle like versus isometric morphology of apatite crystals. *Chemistry of Materials* 13: 1312–1319.

47 Höland, W., Wange, P., Naumann, K. et al. (1991). Control of phase formation processes in glass-ceramics for medicine and technology. *Journal of Non-Crystalline Solids* 129: 152–162.

48 Bohner, M. and Lemaitre, J. (2009). Can bioactivity be tested in vitro with SBF solution? *Biomaterials* 30: 2175–2179.

49 Peitl, O., La Torre, G.P., and Hench, L.L. (1996). Effect of crystallization on apatite-layer formation of bioactive glass 45S5. *Journal of Biomedical Materials Research* 30: 509–514.

50 Plewinski, M., Schickle, K., Lindner, M. et al. (2013). The effect of crystallization of bioactive bioglass 45S5 on apatite formation and degradation. *Dental Materials* 29: 1256–1264.

51 Daguano, J.K.M.F., Rogero, S.O., Crovace, M.C. et al. (2013). Bioactivity and cytotoxicity of glass and glass-ceramics based on the 3CaO–P_2O_5–SiO_2–MgO system. *Journal of Materials Science – Materials in Medicine* 24: 2171–2180.

52 Nommeots-Nomm, A., Houaoui, A., Pradeepan Packiyanathar, A. et al. (2020). Phosphate/oxyfluorophosphate glass crystallization and its impact on dissolution and cytotoxicity. *Materials Science and Engineering C* 117: 111269.

53 Wheeler, D.L., Stokes, K.E., Hoellrich, R.G. et al. (1998). Effect of bioactive glass particle size on osseous regeneration of cancellous defects. *Journal of Biomedical Materials Research* 41: 527–533.

54 Fujibayashi, S., Neo, M., Kim, H.M. et al. (2003). A comparative study between in vivo bone ingrowth and in vitro apatite formation on Na_2O–CaO–SiO_2 glasses. *Biomaterials* 24: 1349–1356.

55 Lindfors, N.C., Koski, I., Heikkilä, J.T. et al. (2010). A prospective randomized 14-year follow-up study of bioactive glass and autogenous bone as bone graft substitutes in benign bone tumors. *Journal of Biomedical Materials Research Part B Applied Biomaterials* 94B: 157–164.

56 Fernandes, H.R., Gaddam, A., Rebelo, A. et al. (2018). Bioactive glasses and glass-ceramics for healthcare applications in bone regeneration and tissue engineering. *Materials* 11: 2530.

57 Gentleman, E., Fredholm, Y.C., Jell, G. et al. (2010). The effects of strontium-substituted bioactive glasses on osteoblasts and osteoclasts in vitro. *Biomaterials* 31: 3949–3956.

58 Jones, J.R., Brauer, D.S., Hupa, L., and Greenspan, D.C. (2016). Bioglass and bioactive glasses and their impact on healthcare. *International Journal of Applied Glass Science* 7: 423–434.

59 Xynos, I.D., Edgar, A.J., Buttery, L.D.K. et al. (2000). Ionic products of bioactive glass dissolution increase proliferation of human osteoblasts and induce insulin-like growth factor II mRNA expression and protein synthesis. *Biochemical and Biophysical Research Communications* 276: 461–465.

60 Hoppe, A., Güldal, N.S., and Boccaccini, A.R. (2011). A review of the biological response to ionic dissolution products from bioactive glasses and glass-ceramics. *Biomaterials* 32: 2757–2774.

61 Massera, J., Mayran, M., Rocherullé, J., and Hupa, L. (2015). Crystallization behavior of phosphate glasses and its impact on the glasses' bioactivity. *Journal of Materials Science* 50: 3091–3102.

62 Iler, R.K. (1979). *The Chemistry of Silica: Solubility, Polymerization, Colloid and Surface Properties and Biochemistry of Silica*. Wiley.

63 Kim, H.-M., Himeno, T., Kokubo, T., and Nakamura, T. (2005). Process and kinetics of bone-like apatite formation on sintered hydroxyapatite in a simulated body fluid. *Biomaterials* 26: 4366–4373.

64 Kansal, I., Goel, A., Tulyaganov, D.U. et al. (2011). Diopside ($CaO{\cdot}MgO{\cdot}2SiO_2$)–fluorapatite ($9CaO{\cdot}3P_2O_5{\cdot}CaF_2$) glass-ceramics: potential materials for bone tissue engineering. *Journal of Materials Chemistry* 21: 16247–16256.

65 Motealleh, A., Eqtesadi, S., Civantos, A. et al. (2017). Robocast 45S5 bioglass scaffolds: in vitro behavior. *Journal of Materials Science* 52: 9179–9191.

66 Sainz, M.A., Pena, P., Serena, S., and Caballero, A. (2010). Influence of design on bioactivity of novel $CaSiO_3$–$CaMg(SiO_3)_2$ bioceramics: in vitro simulated body fluid test and thermodynamic simulation. *Acta Biomaterialia* 6: 2797–2807.

67 Höland, W., Rheinberger, V., Wegner, S., and Frank, M. (2000). Needle-like apatite-leucite glass-ceramic as a base material for the veneering of metal restorations in dentistry. *Journal of Materials Science – Materials in Medicine* 11: 11–17.

68 Höland, W., Ritzberger, C., Apel, E. et al. (2008). Formation and crystal growth of needle-like fluoroapatite in functional glass-ceramics. *Journal of Materials Chemistry* 18: 1318–1332.

69 Müller, R., Abu-Hilal, L.A., Reinsch, S., and Höland, W. (1999). Coarsening of needle-shaped apatite crystals in $SiO_2{\cdot}Al_2O_3{\cdot}Na_2O{\cdot}K_2O{\cdot}CaO{\cdot}P_2O_5{\cdot}F$ glass. *Journal of Materials Science* 34: 65–69.

70 Ritzberger, C., Schweiger, M., and Höland, W. (2016). Principles of crystal phase formation in Ivoclar Vivadent glass-ceramics for dental restorations. *Journal of Non-Crystalline Solids* 432: 137–142.

71 Höland, W., Rheinberger, V., and Frank, M. (1999). Mechanisms of nucleation and controlled crystallization of needle-like apatite in glass-ceramics of the SiO_2–Al_2O_3–K_2O–CaO–P_2O_5 system. *Journal of Non-Crystalline Solids* 253: 170–177.

72 Höland, M., Dommann, A., Höland, W. et al. (2005). Microstructure formation and surface properties of a rhenanite-type glass-ceramic containing 6.0 wt% P_2O_5. *Glass Science and Technology* 78: 153–158.

73 Kasuga, T. (2007). Development of phosphate glass-ceramics for biomedical applications. *Journal of the Ceramic Society of Japan* 115: 455–459.

74 Azenha, M.R., Peitl, O., and Barros, V.M.d.R. (2010). Bone response to biosilicates® with different crystal phases. *Brazilian Dental Journal* 21: 383–389.

75 Moura, J., Teixeira, L.N., Ravagnani, C. et al. (2007). In vitro osteogenesis on a highly bioactive glass-ceramic (Biosilicate®). *Journal of Biomedical Materials Research Part A* 82: 545–557.

76 Kitsugi, T., Yamamuro, T., and Kokubo, T. (1990). Analysis of A·W glass-ceramic surface by micro-beam X-ray diffraction. *Journal of Biomedical Materials Research* 24: 259–273.

77 Kokubo, T., Kushitani, H., Sakka, S. et al. (1990). Solutions able to reproduce in vivo surface-structure changes in bioactive glass-ceramic A-W. *Journal of Biomedical Materials Research* 24: 721–734.

78 Freeman, C.O., Brook, I.M., Johnson, A. et al. (2003). Crystallization modifies osteoconductivity in an apatite–mullite glass-ceramic. *Journal of Materials Science – Materials in Medicine* 14: 985–990.

3

Bioactive Glass S53P4 – From a Statistically Suggested Composition to Clinical Success

Leena Hupa[1] *and Nina C. Lindfors*[2,3]

[1] *Johan Gadolin Process Chemistry Centre, Faculty of Science and Technology, Åbo Akademi University, Turku, Finland*
[2] *Department of Hand Surgery, Helsinki University Hospital, Helsinki, Finland*
[3] *Department of Surgery, Helsinki University, Helsinki, Finland*

3.1 Background

About 50 years after the first scientific publications of bioactive glasses, two compositions dominate the market of clinical products: bioactive glass Bioglass 45S5® discovered by Professor Larry Hench in Florida, USA, and bioactive glass S53P4 developed and widely tested in Finland. This chapter summarizes the road to the clinical applications of S53P4, commercial products based on it, and the current activities for new clinical applications.

3.1.1 Discovery of the Concept of Bioactive Glass and 45S5 Composition

The concept of bioactive glass was introduced in 1971 based on the ability of the glass to chemically bond with the bone after implantation [1]. The bonding developed between the bone apatite and the hydroxyapatite (HAp) crystals that nucleated and grew at the glass surface due to a sequence of dissolution and precipitation reactions *in vivo*. Accordingly, the compositions showing HAp surface layer formation were classified as bioactive glasses. Ideally, the bioactive glasses were thought to react and gradually dissolve in a controlled manner while new bone grows. The subsequent glass dissolution reactions were closely characterized and used to understand tissue-bonding ability [2].

In the beginning, the main focus was on the development of glass compositions that would be suitable prosthesis or graft materials to restore diseased or damaged bone. The first bioactive glasses were composed of four oxides only: SiO_2 as the glass network former, Na_2O and CaO in relatively high contents to provide a composition that would dissolve in aqueous solutions, i.e. extracellular fluid, and some P_2O_5 for the formation of the calcium phosphate compound, HAp [3]. When the bone-bonding and new bone formation mechanisms in the presence of bioactive glasses were explored in more detail, the ion dissolution products of the glass, mainly soluble Ca and Si species, were found to activate and stimulate cellular processes in bone regeneration [3, 4]. The increasing molecular biology knowledge of inorganic ions as activators in the cellular processes turned a new page in developing and understanding bioactive glasses in soft and bone tissue regeneration. Today, bioactive glasses are classified as materials that bond to bone and stimulate bone and soft tissue growth while dissolving over time.

Successful inventions and research outcomes often have a good history behind them. In the well-known review article "The story of Bioglass 45S5®," Professor Larry L. Hench describes how

Bioactive Glasses and Glass-Ceramics: Fundamentals and Applications, First Edition.
Edited by Francesco Baino and Saeid Kargozar.

he discovered the first bioactive glass [3]. Before initiating the search of glasses for prosthetic materials, Professor Hench explored other types of materials, such as radiation-resistant semiconducting glass-ceramics, to be used in satellites. However, a conversation with an Army Medical Corps officer changed his future research efforts to glasses and glass-ceramics for medical applications. The rest is history, and Professor Hench is today recognized as the man behind the new generations of ceramic implant materials, i.e. the bioactive glasses and glass-ceramic for tissue regeneration.

3.1.2 Development of Bioactive Glasses in Finland

The story behind bioactive glass S53P4 is partly similar to 45S5: a meeting with two professors in two different science fields, chemical engineering and medicine, at the two universities in Turku, Finland, in the early 1980s. Professor in Prosthetic Dentistry Antti Yli-Urpo at the University of Turku explored the interactions of metallic restoration materials with porcelain and mucosa [5, 6]. Inspired by the new ideas of bioactive glasses, he asked professor in Inorganic Chemistry Kaj H. Karlsson, a glass scientist at Åbo Akademi University, whether they could together develop glass or glaze coatings suitable on metal prostheses to enhance the tissue adherences (Karlsson, K.H. Personal communication, spring 2021). At that time, Professor Karlsson's research areas included the relationships between glass structure, properties, and oxide composition [7–9]. After this discussion, the interdisciplinary collaboration in bioactive glasses started between the two neighboring universities.

After some preliminary trials, *in vitro* and physical properties of several glass series were tested at Åbo Akademi University. The *in vivo* studies were carried out at the University of Turku and Turku University Hospital. These collaboration projects were financed by the Finnish Technology Agency and the Academy of Finland. The material research goal was to understand the physical and biological properties as functions of the glass oxide composition. These functions would then be used to tailor the most suitable compositions to various clinical needs. The first properties studied included the glass transition temperature, thermal expansion, and water durability [10]. As brittleness of glasses was considered a critical property, the aim was to develop novel compositions for coatings on metals. The glass or glass-ceramic coating should then protect the metal from corrosion and enhance the prosthesis's attachment to bone. Glass transition temperature and thermal expansion described the suitability of the glass to coating processes. Correspondingly, water durability was correlated with the corrosion protection properties. The glasses were directly tested *in vivo* as cylinders drilled in rabbit tibia for eight weeks without any prior *in vitro* testing in buffered solutions. At that time, the protocols and procedures were not as strictly controlled as today, thus, partly explaining the large numbers of rabbit and rat tests done during the early years of bioactive glass research. In total, nine compositions were studied and used as the basis for property modeling. The compositions were statistically chosen in the oxide range (all in wt%) 47.5–68.0SiO_2, 15.2–27.3Na_2O, 8.9–20.6CaO, 2.3–8.9P_2O_5, 0–3.2Al_2O_3, and 0–3.3B_2O_3 to provide a wide range of soluble glasses. The results were then used to express all the properties as functions of the glass composition. An additional goal was to embed the models in a computerized routine for optimizing glass batch compositions to satisfy a selected set of desired properties [11].

3.1.3 Bioactive Glass S53P4 Today

The early studies provided the basis for intensive bioactive glass research in Finland. Research methods and protocols for preclinical and clinical tests were developed and applied for assessing

the suitability of bioactive glasses for the treatment of craniomaxillofacial, dental and orthopedic trauma, tumors, and diseases. Eventually, glass S53P4 became a clinically tested composition in several indications, especially in Finland.

This chapter describes some milestones of Bioactive glass S53P4 on its route to commercial products. Thirty years after the composition was published for the first time, several research efforts are still paid to better understand the physical, *in vitro*, and *in vivo* properties and clinical outcomes of bioactive glass S53P4. Why is this motivated? Dr. Fredrik Ollila, executive chairman and founder of Bonalive Biomaterials Ltd. replied to this question as follows: "Bioactive glass S53P4 performs very well clinically in the currently approved indication areas. However, to be able to solve new clinical challenges, it is helpful to acquire a complete understanding of its properties. All new results enhance our understanding and ensure safe and effective clinical utilization of the bioactive glass S53P4 in current and future applications."

In total, more than 200 scientific papers have been published on the *in vitro*, *in vivo*, preclinical, and clinical studies of bioactive glass S53P4. Also, the glass composition has been discussed in several more papers as a reference composition to new glass formulations. More than 50 papers discuss the *in vitro* properties and physical properties of S53P4. These studies include physical properties of interest for the manufacture of melt-derived products. Noteworthy, the *in vivo* and preclinical studies have been reported in more than 50 papers. The number of clinical case reports and review papers is almost 100, thus indicating the large spectrum of applications tested. This chapter reviews some of the highlights that paved the road to the clinical applications of Bioactive glass S53P4.

3.2 Bioactive Glass S53P4 – From a Concept to First Clinical Trials

3.2.1 The First Series of Glasses, Including S53P4

Among the nine first glasses for bone applications studied in Turku, some showed good bonding to bone, while the bonding was very poor or negligible for some compositions [10]. Based on the results, a new statistical series of 16 compositions was developed within a slightly different range (in wt%): 46–65.5SiO_2, 15–30Na_2O, 11–25CaO, 0–8P_2O_5, 0–3Al_2O_3, and 0–3B_2O_3 [12]. Glass nr. 9 in this series has the composition of 53SiO_2, 23Na_2O, 20CaO, and 4P_2O_5, all in wt%. Today, we know this composition as S53P4, or as Bonalive®, i.e. a commercial product available in different product forms [13].

Unfortunately, no SEM (scanning-electron microscopy)-images have been published of S53P4 in the first *in vivo* study. The desired response, bone bonding, was measured not only for S53P4 but also four other compositions. Two of the compositions did not bind to bone at all, and four had poor contact while five had contact with bone. When examining the history of S53P4, two questions have to be answered: How was the bone bonding defined? Why did the composition S53P4 become the only composition that is used today commercially?

3.2.2 Phenomenological Model of Bone Bonding

The 16 compositions in the glass series were statistically chosen within a wide range to ensure apparent differences in the properties. This approach enabled establishing the limits of bioactivity and gave the basis for numerical modeling of properties as composition functions [12]. The *in vitro* properties, specified as weight loss for grains immersed in Tris-buffer for 6 and 24 hours at 36.5 °C,

varied considerably with the glass composition. The variation was assumed to lead to large differences in the tissue response as well. Then, six cones of each composition were implanted in the rat tibia for eight weeks. The tissue response and the glass surface reactions were evaluated from the cone and surrounding bone cross-sections using SEM imaging and energy-dispersive X-ray spectroscopy (EDS). The EDS line analyses were used to verify whether silica-rich and calcium phosphate-rich (Ca,P) surface layers had formed at the cone surfaces. The glasses showed a wide range of interactions with the bone, ranging from inert compositions to glasses that had bonded to the bone. Poor bone contact was characterized as low *in vitro* solubility combined with a thin or no silica-rich layer at the glass. Three compositions with a high silica content (63.5–65.5 wt%) showed poor bone contact and were thus classified as inert *in vivo*. Five glasses showed bone bonding with distinct silica-rich and Ca,P surface layers. These glasses had high *in vitro* dissolution and were classified as bioactive compositions. The rest of the compositions showed varying bone contact degrees, silica-rich layer and Ca,P-layer thicknesses.

The results were used to establish a phenomenological model of *in vivo* bone bonding, expressed as the reaction number, RN. The weight loss *in vitro*, *in vivo* formation of silica-rich and Ca,P-layers, and bone contact type were evaluated for each composition. Based on these characteristics, the glasses were divided into groups with numerical values from 1 to 6. Group 1 glasses had low weight loss, no or negligible layers and no bone contact, while group 6 glasses showed high weight loss, distinct silica-rich and Ca,P-layers, and chemical bonding to bone [12]. The other behavior combinations gave the numbering for the other glass groups. The developed RN-model expresses the bioactivity as a function of the composition of the glass in wt%. For a glass to be bioactive, the RN value should be higher than 5:

$$\mathrm{RN} = 88.3875 - 0.011\,627\,2[\mathrm{SiO_2}]^2 - 0.980\,188[\mathrm{Na_2O}] - 1.123\,06[\mathrm{CaO}] - 1.205\,56[\mathrm{P_2O_5}] - 0.056\,052\,7[\mathrm{B_2O_3}]^2 - 2.086\,89[\mathrm{Al_2O_3}]$$

The model was not verified with other compositions and not used to computerize new compositions. The calculated RN value for the original bioactive glass 45S5 by Professor Hench well satisfies the bioactivity criterion. Later, the model has been shown to work with some other compositions. However, the lack of other alkali or alkaline earth oxides than Na_2O and CaO limits the RN model's usability range [14].

3.2.3 *In Vivo* Bone Bonding vs. Glasses with Al_2O_3 and P_2O_5

Alumina's role on the bone bonding was studied in more detail with a few compositions selected from the series of 16 glasses. As the glasses with the highest alumina contents had not shown bone bonding, six compositions containing 0–3 wt% Al_2O_3 and one reference titanium cone were implanted in rabbit tibia, and the push-out strength of the implants was measured after six weeks. All three cones with 2.5 or 3 wt% Al_2O_3 showed low push-out strengths, also, if the cones had a Ca,P surface layer [15]. Thus, the formation of Ca,P surface layer *in vivo* was not a sufficient bone-bonding criterion. Earlier *in vitro* studies of alumina-containing glasses in Tris-buffer had shown that aluminum was enriched in the silica-rich layer and interfered with the formation of calcium phosphate surface layer [16]. Alumina in the Ca,P layer was thus assumed to prevent the implant's proper chemical bonding to bone.

In an another early *in vivo* study, two other bone bonding compositions than S53P4 from the same glass series were selected to study the impact of P_2O_5 in the glass on the initial stage of calcium phosphate formation on the glass surface. After eight weeks in rat tibia, both the composition without

and with 4 wt% P_2O_5 showed good bone bonding [17]. The results showed that the migration of phosphate from the glass is not a prerequirement for bonding to bone. The hydrated silica gel's flexible structure at the surface provides nucleation sites for phosphate ions from the physiological solution.

Alumina-free, bone-bonding compositions were selected for further *in vivo* studies and clinical tests. Two of the glasses in the series of 16 glasses fulfilled these criteria: S53P4 and S46P7. The latter contains 46 wt% SiO_2 and 7 wt% P_2O_5 and is thus close to 45S5 composition. Based on the first trials' clinical outcome [18, 19], S53P4 became the composition that was tested using several animal models for various potential clinical applications.

3.2.4 Soft and Hard Tissue Bonding *In Vivo*

The first *in vivo* studies of S53P4 in soft tissue of rabbits and hard tissue in sheep were reported in 1994 [20]. Granules of the glass were implanted in muscle and connective tissue of rabbit and mandibular bone of sheep. Similar reactions were reported after two to three months in all three implantation sites: silica-rich layer with calcium phosphate precipitates. In soft tissues, large precipitates with a composition close to apatite were analyzed. The molar ratio Ca:P suggested that the Ca,P precipitation in the silica-rich layer originated from the ions released from the glass. Correspondingly, the Ca:P-ratio in the surface apatite implied phosphate incorporation from the physiological environment. Figure 3.1 shows an SEM image of an S53P4 granule surrounded by new bone after the implantation in the sheep jaw. The EDS analyses of the points shown in the SEM image are listed in Table 3.1. A silica-rich layer with increasing P_2O_5 content (Pts 3–5) surrounds the granule core with a composition close to the original glass (Pt 1). The Ca/P molar ratios are almost similar in the outermost granule layer (Ca/P = 1.4 in Pt 6) and the new bone (Ca/P = 1.3 in Pt 7), thus verifying chemical bonding between them [20].

3.2.5 *In Vivo* Evidence of S53P4 in Bone Healing

In one early *in vivo* study, bioactive glass S53P4 granules were compared with polytetrafluoroethylene (PTFE) membrane to repair cortical bone defects in rabbit tibia [21]. After 6 and 12 weeks, a markedly better bone repair was obtained when using the bioactive glass than PTFE or empty control defects. The new bone that grew along the bioactive glass granules formed a continuous bridge over most defects, as shown in Figure 3.2.

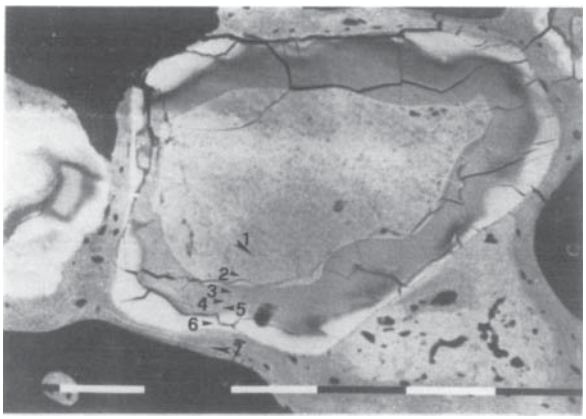

Figure 3.1 SEM micrograph of an S53P4 granule implanted in a sheep's mandibular bone. The numbers indicate the points of the EDS analyses in Table 3.1. The bar equals 100 µm. Source: Gatti et al. [20]/with permission from Elsevier.

Table 3.1 EDS analyses of the degrading S53P4 granule (Pt 1–6) and the surrounding bone in Figure 3.1 (Pt 1 and 2 glass, Pt 3–4 silica rich layer, Pt 6 Ca,P layer, Pt 7 bone).

	Pt 1	Pt 2	Pt 3	Pt 4	Pt 5	Pt 6	Pt 7
SiO_2	49.2	50.2	76	70.5	64.7	2	0.9
Na_2O	20.1	20	0.3	0	0	0.5	0.5
CaO	19.5	10.5	7.9	9.5	9.9	45.5	39.9
P_2O_5	4.2	4.2	5.5	7.2	7.8	32.2	30.5
Total	93	94	89.9	87.5	82.8	81	72.9

Source: Gatti et al. [20]/with permission of Elsevier.

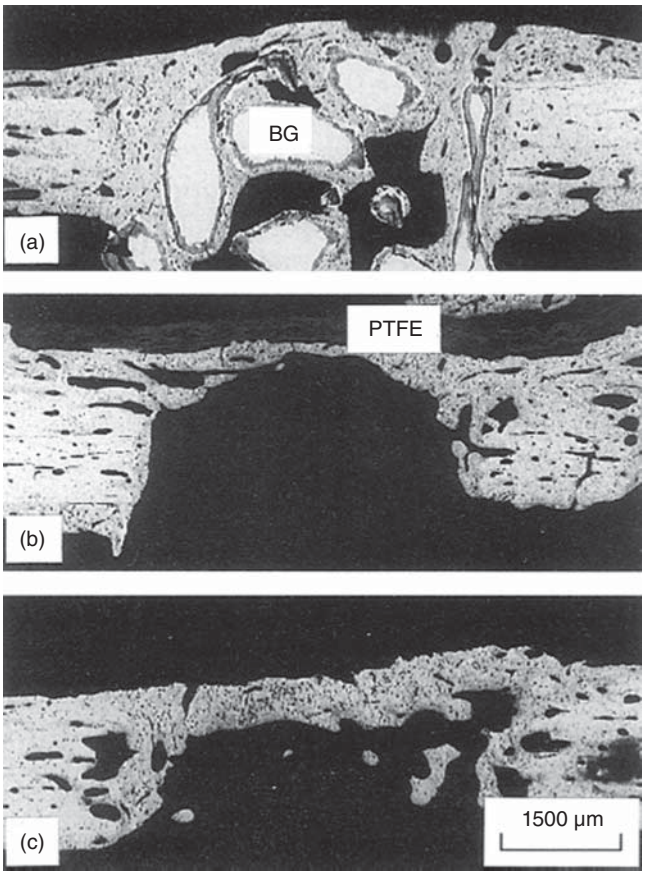

Figure 3.2 SEM images showing defect closure in rabbit tibia after six weeks for (a) defect filled with S53P4 granules, (b) defect covered with polytetrafluoroethylene membrane, and (c) empty control defect. Source: Turunen et al. [21]/with permission from Springer Nature.